

Spatial and temporal distribution of hailstorms in the Alpine region: a long-term, high resolution, radar-based analysis

L. Nisi,^{a,b,c,d,*} O. Martius,^{a,b,c} A. Hering,^d M. Kunz^e and U. Germann^d

^aOeschger Centre for Climate Change Research, University of Bern, Switzerland

^bInstitute of Geography, University of Bern, Switzerland

^cMobililar Lab for Natural Risks, University of Bern, Switzerland

^dFederal Office of Climatology and Meteorology MeteoSwiss, Locarno-Monti, Switzerland

^eInstitute of Meteorology and Climate Research (IMK), Karlsruhe Institute of Technology (KIT), Karlsruhe, Germany

*Correspondence to: L. Nisi, Via ai Monti 146, 6605 Locarno-Monti, Switzerland. E-mail: luca.nisi@meteoswiss.ch

This article presents a 13-year hail climatology for Switzerland based on volumetric radar reflectivity. Two radar-based hail detection products that are used operationally at MeteoSwiss, namely the Probability of Hail (POH) and the Maximum Expected Severe Hail Size (MESHS), have been reprocessed for the extended convective season (April–September) between 2002 and 2014. The result of these two products is a comprehensive hail distribution map, which highlights regional and local-scale hail characteristics. The map of the annual number of hail days shows a high spatial variability and several maxima over the foothills north and south of the Alps as well as over the Jura mountains. Directly over the Alps hail frequency exhibits a minimum. Annual hail anomalies show a pronounced variability, which suggests that hail occurrence is strongly controlled by large-scale weather patterns. Furthermore, hail probability exhibits a strong seasonal and diurnal cycle with a maximum in July in the late afternoon. The hail peak over the northern pre-alpine region occurs approximately two hours earlier compared to the south. A possible explanation is the trigger mechanism between the cold pool initiated by early convective cells over the Jura mountains and the development of cells on the northern slope of the Alps. Since radar-based hail signals are only indirect measurements, statistical verification of the hail detection algorithms is crucial. Damage reports from an automobile insurance company are used as an independent dataset. Verification results confirm that radar-based hail algorithms provide valuable information on hail probability. Finally, the synoptic-scale hail-driving weather conditions are investigated using a weather type classification based on upper-air flow direction and mean pressure from a numerical weather prediction model. The results show that six out of nine main synoptic-scale patterns favour the development of hailstorms in Switzerland.

Key Words: hail; hailstorms; convection; weather radar; Switzerland; diurnal cycle

Received 7 September 2015; Revised 27 December 2015; Accepted 19 February 2016; Published online in Wiley Online Library 30 March 2016

1. Introduction

Hail has been a subject of scientific interest for many decades (e.g. Plumandon, 1901; Changnon, 1978) because of the severe damage it causes to agriculture, buildings and cars. For a specific location, hail is a low probability high impact weather event (e.g. Delobbe and Holleman, 2006). Hail is characterized by a strong local-scale variability of the occurrence and intensity, and the small extent of the affected areas referred to as hailstreaks (e.g. Weisman *et al.*, 1997; Bryan *et al.*, 2003; Sánchez *et al.*, 2013). As a consequence, point observations of hail are not representative for larger areas. Compared to other atmospheric parameters such as temperature

or precipitation, observational networks need to be at least ten times denser to capture all hailstreaks (Wieringa and Holleman, 2006). Physical measurements collected with dense networks are an ideal basis to investigate multi-year hail occurrence, hail variability and hail trends. Additional information is provided by reports from trained storm spotters or newspapers, which are archived in different databases, for example the European Severe Weather Database (ESWD). Several hail climatologies and analyses have been compiled worldwide during the last decades based on data from human or automatic observations (e.g. Changnon, 1978; Changnon and Changnon, 2000; Xie *et al.*, 2008, 2010; Zhang *et al.*, 2008; Tuovinen *et al.*, 2009; Mezher *et al.*,

2012) and hailpads (e.g. Dessens and Fraile, 1994; Sánchez *et al.*, 1996, 2013; Eccel and Ferrari, 1997; Dessens *et al.*, 2001; Vinet, 2001; Fraile *et al.*, 2003; Giaioti *et al.*, 2003; Počakal *et al.*, 2009; Berthet *et al.*, 2011; Manzato, 2013).

Unfortunately, only a few dense hail-observation networks exist worldwide (e.g. in several parts of France or northern Italy), and Switzerland does not have a ground-based hail observation network. For this reason, studies on hail occurrence require indirect observations, primarily radar data or insurance loss data.

Weather radar-based hail detection algorithms can be useful for investigating hail frequency over larger areas (e.g. Basara *et al.*, 2007; Cintineo *et al.*, 2012) and in regions where long observation time series, like in Switzerland, do not exist. Hail detection by weather radar has a long history. In the fifties, first studies were conducted to investigate the presence of hail in thunderstorms by means of weather radars (e.g. Donaldson, 1961). A series of studies analysed the relation between the presence of hail and different radar parameters such as: vertical reflectivity profiles (Wilk, 1961), height of strong echoes (e.g. Douglas, 1963), maximum reflectivity (e.g. Rinehart *et al.*, 1968), height of the 45 dBZ contours in storm profiles (Mather *et al.*, 1976), height difference between the 45 dBZ reflectivity and the melting layer (Waldvogel *et al.*, 1979), or vertical integrated liquid water (e.g. Amburn and Wolf, 1997). Several radar-based methods for estimating the probability of hail (e.g. Waldvogel *et al.*, 1979), the hail kinetic energy (e.g. Sánchez *et al.*, 2013) and the maximum expected hailstone size (e.g. Treloar, 1996; Edwards and Thompson, 1998; Witt *et al.*, 1998) were developed and implemented operationally by weather offices. Summaries of the most commonly used hail detection techniques using single-polarization C-band radars are presented in Holleman (2001), Sánchez *et al.* (2013) and Kunz and Kugel (2015).

Insurance loss data usually have a high spatial coverage and are available over a long period, but are affected by several sources of uncertainty (e.g. Willemse, 1995; McMaster, 1999; Changnon *et al.*, 2001; Webb *et al.*, 2001a; Schuster *et al.*, 2005; Kunz and Puskeiler, 2010). They are strongly dependent on non-meteorological characteristics like population density, object vulnerability and claim handling (Dessens *et al.*, 2009; Mohr and Kunz, 2013). According to Vinet (2001), damage observations are the results of the combination of 'object vulnerability' (property) and 'agent risk' (hail). Nevertheless, these datasets provide one of the few possibilities for cross-validating radar-based hail observations in areas where ground-based hail observation networks are not available. For example, Kunz and Kugel (2015) and Skripniková and Řezáčová (2014) used building loss information for validating and adjusting radar-based hail detection algorithms.

Switzerland is regularly affected by severe hailstorms causing substantial damage. Despite the high hail risk exposure, only a few climatological hail investigations based on insurance and radar data exist (e.g. Houze *et al.*, 1993; Willemse, 1995; Stucki and Egli, 2007). Substantial improvements of the Swiss radar network offer the unique opportunity to extend and broaden the existing knowledge. Long-term information on hail occurrence is not only relevant for agriculture and the insurance industry, but also serves as a basis for the advancement of hail forecasting in Switzerland. Building on climatological knowledge of the temporal and spatial distribution of hailstorms allows assessment of the hail hazard and hail risk for different regions (Wieringa and Holleman, 2006).

Forecasting severe storms is a challenging task due to the chaotic nature of convective processes. In particular over complex orography, high spatial and temporal gradients make the task of observing and nowcasting thunderstorms challenging (e.g. Mecklenburg *et al.*, 2000; Hering *et al.*, 2004; Rotach *et al.*, 2009; Mandapaka *et al.*, 2012; Nisi *et al.*, 2014). However, in mountainous areas the orographic forcing is a source of repeatability of precipitation and convective cells (Foresti *et al.*, 2011), and knowledge about hail occurrence in the past is very valuable for many applications.

The aim of this study is to investigate the distribution of hail over Switzerland and adjacent regions, which are characterized by complex terrain and the absence of hail detection networks (e.g. hailpads). Hail occurrence is assessed by using radar-based observations (full resolution) over a 13-year investigation period. Volumetric radar data from the Swiss radar network are combined with information from the regional numerical weather prediction (NWP) model Consortium for Small-scale MOdelling (COSMO-CH). Two operational single-polarization hail detection algorithms are reprocessed for the extended convective season (April–September) between 2002 and 2014. The results are analysed to address the following questions: (i) What is the annual, monthly and hourly distribution of hail occurrence over the pre-alpine and alpine regions? (ii) Is it possible to identify and characterize the synoptic-scale hail-favouring weather conditions? (iii) Does the application of radar-based hail detection algorithms over a region with complex terrain yield reliable results?

2. Domain and datasets

2.1. Investigation area

The region under investigation has a complex orography, characterized by deep valleys with lowest altitude around 100 m above sea level (a.s.l.) and mountains with peaks above 4000 m a.s.l., see Figure 1. We considered in the analysis both the whole domain and smaller sub-regions, see orange areas in Figure 1. The six sub-regions exhibit different terrain as well as climatological conditions. The Jura (1) is a long south-west to north-east oriented mountain ridge, the highest peak of which is the Crêt de la Neige at 1720 m a.s.l. The northern slopes of the Alps (2) encompass a mixture of flat and hilly terrain (Swiss Plateau) and mountainous regions (Pre-alps) with an average altitude of 580 m a.s.l. and peaks reaching 1500 m a.s.l. The Alps (3) are characterized by deep valleys and high peaks with altitudes ranging between 400 and more than 4810 m a.s.l. The southern pre-alpine area (4) is dominated by hilly terrain. Finally the Po valley (Italy; 5) is characterized by flat terrain, and the federal state of Baden-Württemberg (Germany; 6) encompasses a mixture of flat and hilly terrain (Black Forest).

2.2. Radar data

In this study two C-band Doppler radars from the MeteoSwiss radar network have been used, that is Albis and Monte Lema (Figure 1). For reasons of data homogeneity, data from the third radar on La Dôle was not included; rather the maximum range used in this study is 160 km. Starting from June 2011, the C-band Doppler radar network (Joss *et al.*, 1998) has been completely renewed and extended adding dual-polarisation capability and two additional radar sites to improve coverage in the inner-alpine regions (Germann *et al.*, 2015). This is the fourth generation of weather radars in Switzerland. Details on third and fourth generation radar data processing are described in Joss *et al.* (1998) and Germann *et al.* (2015). The calibration is performed with an internal noise source generator every 5 min, whereas an external calibration using the Sun is performed on a daily basis.

To calculate the Probability Of Hail (POH) and the Maximum Expected Severe Hail Size (MESHS), the 45 and 50 dBZ echo top height products are used (ET45 and ET50 hereafter). ET45 and ET50 represent the highest altitude at which a radar reflectivity of at least 45 and 50 dBZ, respectively, can be detected (Donaldson, 1961). The parameters ET45, ET50, POH and MESHS are two-dimensional, gridded Cartesian products. For more details see Table 1. For many years echo top height products have been used for the diagnosis of severe convection (e.g. Held, 1978; Waldvogel *et al.*, 1979; Witt *et al.*, 1998) and for radar-based thunderstorm nowcasting systems (e.g. Dixon and Wiener, 1993; Johnson *et al.*, 1998; Hering *et al.*, 2008). Quantitative radar estimation

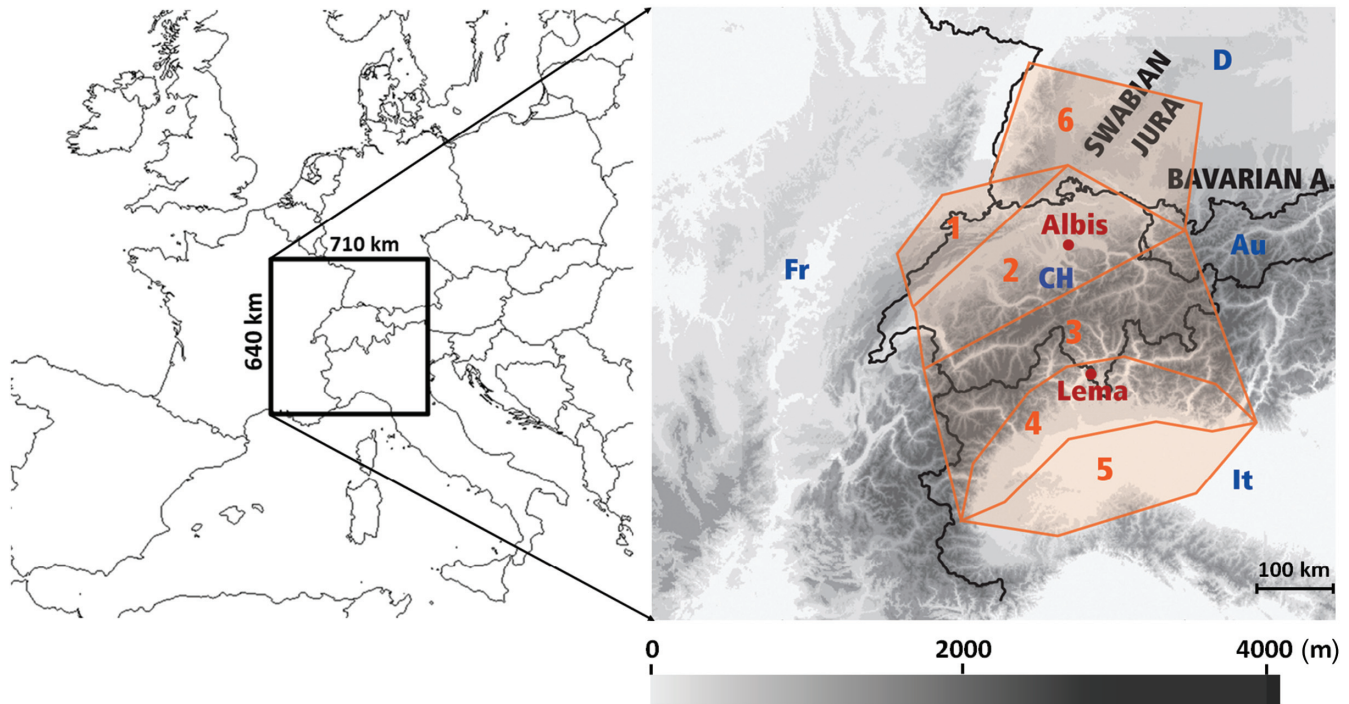


Figure 1. Investigation area and the six sub-regions analysed in this article (1: Jura; 2: Northern Pre-alps; 3: Alps; 4: Southern Pre-alps; 5: Po valley; 6: Baden-Württemberg). Red dots indicate the location of the two radars used in this study. CH: Switzerland; D: Germany; Fr: France; It: Italy; Au: Austria.

Table 1. Specifics of the third and fourth Swiss radar generation and related product resolutions.

	Before June 2011	In between	After June 2012
Radar generation	Third	Transition phase	Fourth
Radar capabilities	Doppler		Doppler + polarimetric
Radar resolution (polar data)	1 km × 1°		500 m × 1°
Spatial resolution of Cartesian products	2 × 2 km ²		1 × 1 km ²
Scan strategy	20 elevations (−0.3° to +40°) repeated every 5 min		20 elevations (−0.2° to +40°) repeated every 5 min

of precipitation over complex terrain has to cope with several major challenges (see section 3.5).

2.3. Freezing-level height from the regional NWP model COSMO-CH

The radar-based hail detection algorithms POH and MESHS require information on the freezing-level height (hereafter H0). This information is extracted from COSMO-CH analysis (<http://cosmo-model.org/>). COSMO-CH is a non-hydrostatic, regional, high-resolution numerical weather prediction model operated by MeteoSwiss. The horizontal resolutions are 6.6 × 6.6 km² (COSMO-7) and 2.2 × 2.2 km² (COSMO-2), respectively, and the temporal resolution is 1 h.

H0 represents the model grid-cell where the three-dimensional (3D) temperature field is equal to 0 °C. During the investigation periods, the model set-up changed over time. Between March 2002 and March 2008 only one model resolution was available with a 7 × 7 km² mesh-grid, whereas after March 2008 both COSMO-7 and COSMO-2 were available. Another minor change concerns the algorithm for the diagnosis of the freezing level. The bottom-up algorithm was substituted with a top-down approach in May 2011. This modification had a significant effect during stable situations with a temperature inversion only, but no effect in the case of convective events.

The sensitivity of POH (or MESHS, respectively) to errors in the definition of H0 decreases with increasing difference between ET45 (or ET50, respectively) and H0. For example, an H0 error of ±1000 m produces a variation in POH of ±20–40% if POH < 60% and ±10–20% if POH ≥ 60%. For MESHS the

variation is more linear and corresponds to ±1 cm for all hail sizes. An H0 error of a few hundred metres produces a small variation only, for both POH and MESHS. A statistical verification of upper-air temperature shows a bias smaller than 1 °K. Consequently the bias of H0 is small as well (<100 m). However, local precipitation dynamics inside the model have to be considered. Latent energy from melting and evaporation processes affects H0 especially in the case of intensive convective rain. These physical processes are parametrized in the model. Such small-scale effects on H0 were not considered in the calibration of hail products when proximity soundings were used (Waldvogel *et al.*, 1979; Treloar, 1998; Joe *et al.*, 2004). This may have a consequence causing overestimation of hail (M. Stoll, MeteoSwiss, 22 November 2015; personal communication). However, this process causes a decrease of H0 of several hundred metres only in rare cases. Therefore, we neglected this effect in this study, given the low sensibility of POH and MESHS to changes in H0.

2.4. Weather type classification

Recently a new automatic weather type classification method (hereafter WTC) has been introduced at MeteoSwiss (Weusthoff, 2011). On a daily basis, ten classifications based on two different methods (GrossWetterTypes, GWT, and Cluster Analysis of Principal Components, CAP) are calculated. WTCs have been calculated using reanalysis data of ERA40 (Uppala *et al.*, 2005) and ERA-Interim (Dee *et al.*, 2011) back to 1957 and stored in the MeteoSwiss database. In this study we used a ten-member classification with predefined weather types based on geopotential, mean wind speed and direction at 500 hPa (Table 2).

Table 2. The ten members of the weather types classification used in this study.

Type	Description
WT1	Westerly
WT2	Southwesterly
WT3	Northwesterly
WT4	Northerly
WT5	Northeasterly
WT6	Easterly
WT7	Southeasterly
WT8	Southerly
WT9	Low pressure
WT10	High pressure

Adapted from Weusthoff (2011).

2.5. Insurance loss reports used for verification

The results of the two applied hail detection methodologies were validated using hail loss data (cars) from a major insurance company in Switzerland. In this study, car losses collected over a 10-year period (2003–2012) were used. Daily damage locations and frequency are provided for each municipality in Switzerland (four-digit postal code zones, 3195 in total). The average area per postal code is 12.9 km². Note however, that in mountainous and rural regions postal code zones may be much larger. On the other hand, cities encompass several postal codes with smaller areas.

The insurance datasets were corrected manually in order to eliminate obvious errors due to the recording procedure (e.g. elimination of single claims on days and over regions without observed rain; see Morel (2014) for more details).

The relation between hail kinetic energy and automobile losses in Switzerland was studied by Hohl *et al.* (2002). They show that losses grow exponentially with hail size. However, it is difficult to determine a size threshold for damaging hail. Indeed, several factors like car structure, hailstone geometry, hailstone density, presence of rain, impact angle, horizontal velocity and other meteorological and non-meteorological factors can affect the extension and the amount of damage. Hohl *et al.* (2002) found that in general hailstones with diameters larger than 2 cm produce substantial damage to automobiles.

3. Methods

3.1. Probability of hail (POH)

Waldvogel *et al.* (1979) investigated and verified radar-based hail detection criteria over Switzerland. They presented a methodology, which considers the vertical distance between ET45 and H0 as an indication for the presence of hailstones on the ground:

$$\Delta z = ET45 - H0 \geq 1.4 \text{ km.} \quad (1)$$

In this formulation, the height difference Δz in Eq. (1) is a proxy for the zone where hail may grow by riming in deep convective storms. The success of this algorithm was further confirmed by other authors, who were mainly involved in hail suppression experiments (e.g. Foote and Knight, 1979). Later Witt *et al.* (1998) showed that this criterion is useful for estimating the hail probability (POH). For this purpose, they considered the distance Δz to be proportional to the probability of hail on the ground. POH provides an estimate of the presence of hail of any size at the ground, with a scale ranging from 0 (no hail; $\Delta z < 1.65$ km) to 100% (hail; $\Delta z > 5.5$ km). Several versions of the technique proposed by Waldvogel *et al.* (1979) have been tested extensively in different countries showing that it provides reasonable results for single-polarisation radar data (e.g. Kessinger *et al.*, 1995; Holleman, 2001; Delobbe and Holleman, 2006; Skripniková and Řezáčová, 2014). Furthermore, the algorithm

has been implemented operationally by several weather services (e.g. Witt *et al.*, 1998; Holleman, 2001; Šálek *et al.*, 2004; Betschart and Hering, 2012) and adjusted for different purposes (e.g. Puskeiler, 2013; Kunz and Kugel, 2015). The version proposed by Foote *et al.* (2005), tested for a C-band radar, has been used operationally at MeteoSwiss since 2008 and is used in this study.

3.2. Maximum expected severe hail size (MESHS)

Radar-based approaches have also been employed for estimating the hailstone size. Treloar (1998), for example, empirically investigated the relation between some radar and upper-air parameters. A few years later, an empirical algorithm based on the work of Treloar (1998) was implemented and run operationally during the Sydney 2000 Forecast Demonstration project (Joe *et al.*, 2004). The algorithm provides a reasonable estimation of the maximal hailstone size on the ground using the relation between the height of ET50 and H0. It was successfully tested for monitoring severe hailstorms during the Olympic games in 2000 (Webb *et al.*, 2001b). The algorithm implemented operationally at MeteoSwiss was empirically derived from Fig. 3 in Joe *et al.* (2004). It has been used since 2009 for both warning purposes and climatological analyses. The algorithm estimates the maximal size of hailstones at the ground for hailstone diameters equal to or larger than 2 cm, which is the critical size for damage to buildings or automobiles. MeteoSwiss verified the information provided by the MESHS product using ground-truth hail reports collected from the media over a limited period (Betschart and Hering, 2012). Because of the lack of large and reliable datasets of hailstone sizes, performing a solid verification of the algorithm is not possible at the moment. For this reason, hail analyses presented in this article are mainly based on POH.

3.3. Creating a multi-year POH and MESHS dataset

A 13-year period was selected, from 2002 till 2014. The period has been selected such that the quality of input data from radar and COSMO-CH is fairly high and homogeneous, and the number of hail cells in the domain is sufficiently large to calculate frequency statistics at the desired space–time resolution. POH and MESHS have been reprocessed for the 13 extended convective seasons from April to September using data from COSMO-CH and over 27 million scans from the two radars Albis and Lema, see Figure 1. Polar third-generation data have been interpolated to the fourth-generation polar data. The same value of a 1000 m third-generation bin has been assigned to two 500 m bins simulating fourth-generation polar data. For the whole investigation period radar outages were below 4%. Outage times were mainly due to ordinary maintenance and mostly during fair weather conditions in the absence of precipitation. Reprocessing was necessary to account for changes in the spatial resolution of COSMO-CH and the scan program and data format of the new fourth-generation radar network. The goal of the reprocessing was to obtain a homogeneous database suitable for the investigation of spatial and temporal patterns in the hail distribution over Switzerland. For more details see Figure 2.

3.4. Hail days and anomalies

Daily POH and MESHS products were quantified from the respective maxima of the 5 min values at every grid point. From these fields the number of hail days per season (Figures 4 and 5) and the number of hail days per month (Figure 7) are determined. For each grid point, a hail day is defined either as POH > 80% (Figures 4, 7, 10 and 11), or MESHS > 2 cm or MESHS > 3 cm or MESHS > 4 cm (Figure 5). The 80% POH threshold is selected based on (i) statistical verification with insurance loss data (section 4.5) and (ii) the evaluation of the applicability of radar-based hail algorithms over the Alps (section 3.5). The diurnal cycle is computed using the normalized average hourly hail frequency

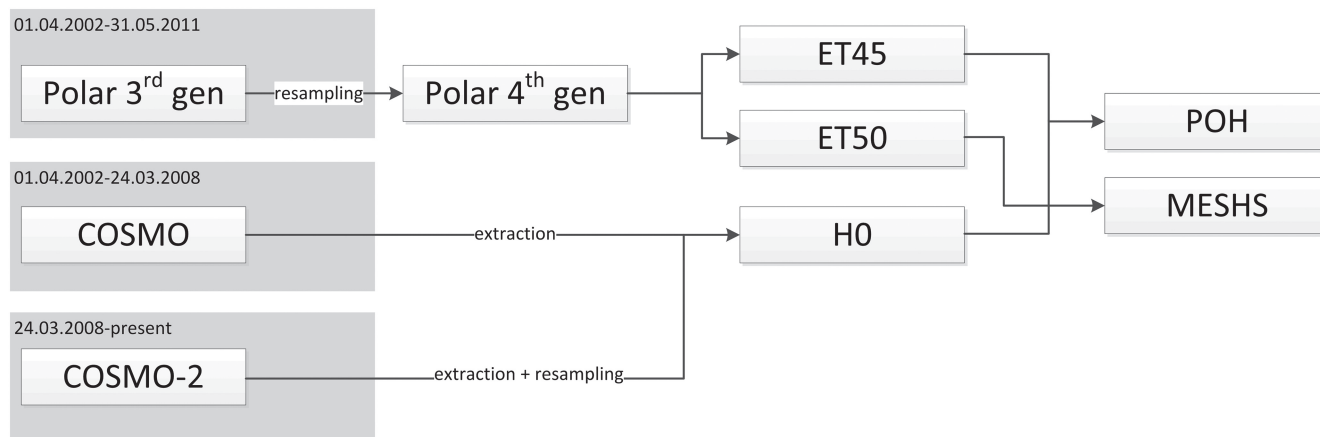


Figure 2. Reprocessing strategy for creating long-term, homogenous POH and MESHS datasets.

(Figure 9). For each grid point, a ‘hail hour’ is considered when $POH > 80\%$. Standardized anomalies N (Wilks, 2006) are used to discuss annual hail variability over Switzerland (Figure 6):

$$N = \frac{p_i - \mu}{\sigma}, \quad (2)$$

where p_i is the hail frequency of the i th year, μ is the mean over several years, and σ is the standard deviation (hereafter STD).

3.5. Discussion of radar-based approaches over complex terrain

As opposed to all other hail observing systems, a radar offers a unique capability to simultaneously observe hail cells down to the size of a few square kilometres and minutes over a large domain. However, some challenges which can affect the quality of the data must be discussed. Among them we find ground clutter and bright-band contamination, partial beam blocking, beam shielding, overshooting and widening as well as different attenuation effects (e.g. Joss *et al.*, 1998; Germann *et al.*, 2006; Villarini and Krajewski, 2010; Mandapaka *et al.*, 2013). Over complex terrain like the Alps some of these effects (e.g. beam shielding) may severely modify the observations, see for instance Germann *et al.* (2006). Bright-band contamination and beam overshooting only marginally affect POH and MESHS. The former, a local increase in reflectivity due to the melting of frozen hydrometeors, is an effect that is mainly relevant for stratiform precipitation, but not for convective cells. Even if occasionally the bright band may produce reflectivity values larger than 45 dBZ at the altitude of the freezing level, the difference in height between ET45 and H0 is too small to affect the identification of hail by radar, see Eq. (1). Furthermore, beam overshooting, increasing with the distance off the radar, also affects both hail algorithms only marginally. The criteria for a positive detection by POH and MESHS require the ET45 and the ET50 to be located at mid- and high levels of the troposphere. For example, assuming a freezing level at 3000 m, ET45 has to be 7200 m for a POH value of 80%. In such cases, beam overshooting does not play a role. Only during the early convective season (April–May), when usually air-mass conditions limit the vertical development of convective cells to around 6000–8000 m and when the freezing level is still low, beam overshooting can be an issue. The spatial distribution of the hail signals, however, is mainly governed by the events during June and July (cf. Figure 7), where the effect of beam overshooting is negligible.

The other three issues, namely ground-clutter contamination, partial and total beam shielding and different types of attenuation, may affect the hail products. MeteoSwiss uses a sophisticated clutter suppression algorithm, based on Doppler and statistical filtering (Joss *et al.*, 1998), which is continuously improved (Germann *et al.*, 2006, 2015) and eliminates clutter efficiently. In the fourth-generation radar data, residual clutter is a marginal

issue. In the third-generation radar data a few clutter pixels remain near to mountain peaks. However, the effect on the hail products is negligible because these radar echoes are located at lower altitudes and do not result in high echo-tops used as criteria for hail.

A particular type of clutter occurs in inversions with anomalous propagation. The impact on the hail studies is negligible because anomalous propagation is unlikely in convective situations and limited to low altitudes.

Wet-radome attenuation affects the data used in this study only marginally. The concomitant occurrence of convective storms exactly over the radar site and the presence of hailstorms in the radar domain is rare. Based on our dataset less than 0.2% of all thunderstorms are affected. Non-convective rain on the radar site is more frequent, but here the resulting attenuation is limited to a few decibels (Germann, 1999).

Path attenuation can have an effect on hail data when a hailstorm is located behind intense precipitation. Statistically speaking this applies only to a few hailstorms in our dataset. At current status MeteoSwiss is testing an attenuation correction algorithm using polarimetric data of the fourth generation.

Beam widening is another potential error in radar applications. This effect increases with the distance between the radar site and the location of the scatterer (e.g. Cintineo *et al.*, 2012). In order to minimize this effect a two-radar composite has been used and the maximum range has been reduced to 160 km.

Partial beam blocking is another challenge especially in complex topography. MeteoSwiss computes the visibility of each pixel of the domain from a digital terrain model. Based on the visibility, partial beam blocking is corrected at the level of the polar data.

Beam shielding by obstacles and mountain ranges has a direct influence on the altitude of the lowest radar beam. These altitudes are particularly high over mountain ranges and over areas behind higher mountains that are covered only by a single radar. By means of a worst-case example, Figure 3 shows the altitude of the lowest visible beam of the Monte Lema radar. Because of the shielding of a nearby mountain peak the altitude of the lowest radar beam towards the northeast exceeds 8 km at a distance of 150 km.

Taking profit from a two-radar composite and limiting the radius to 160 km, the altitudes of the lowest radar beams over the Alps are generally below 5000 m. Over a limited area in the central Alps they range between 5000 and 6700 m. POH values of 40, 60 and 80% correspond to Δz differences (see Eq. (1)) of 2400, 3070 and 4200 m, respectively (Foote *et al.*, 2005). If a typical summertime freezing level located around 3000 m is considered, issues arise in locations where the altitude of the lowest radar beam exceeds 5400, 6070 and 7200 m (for POH of 40, 60 and 80%, respectively). Since for all the presented investigations a POH threshold of 80% has been used, the shielding issue can be neglected. Evidently, by decreasing the freezing-level

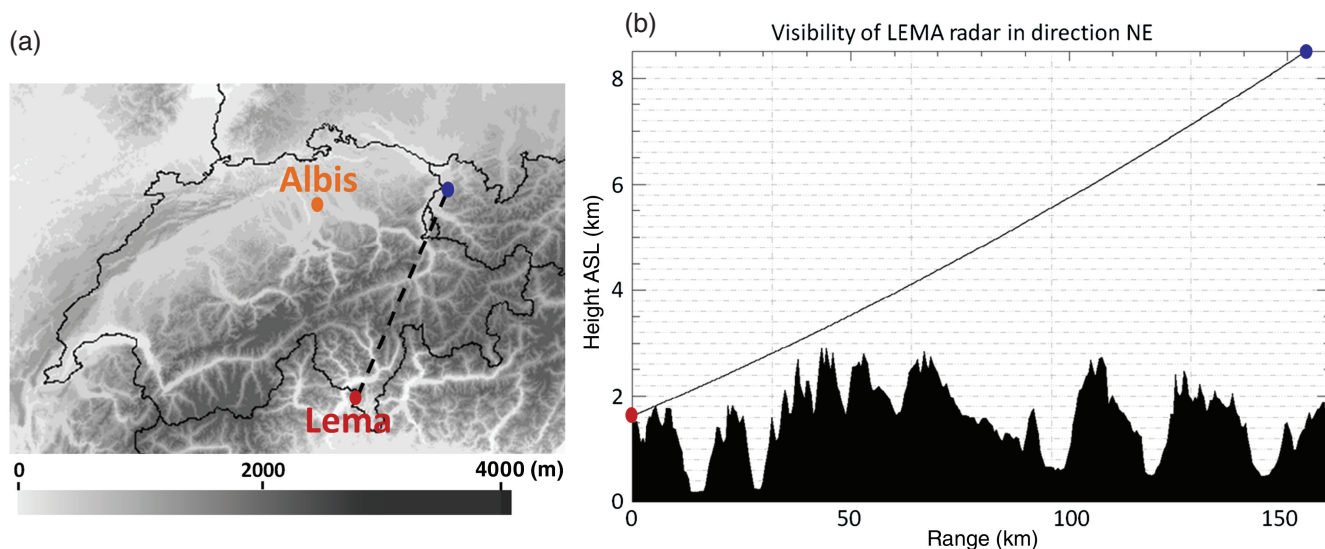


Figure 3. In the direction of north-northeast the beam of the Lema radar is severely shielded by a nearby mountain (a). At a distance of 150 km the radar can observe precipitation only at a height of 8 km and higher (b). This is the direction with most severe shielding. The position of the Albis radar is also shown.

height and the POH threshold, this issue may become more relevant.

Generally speaking, it can be concluded that POH and MESHS are calculated using radar reflectivities at high altitudes. For this reason, they are less affected by radar issues which typically affect quantitative precipitation estimation near the ground.

3.6. Verification

The algorithms employed in this study are validated against insurance claim reports by the method of categorical verification, which is widely applied in meteorology (e.g. Delobbe *et al.*, 2003; Saltikoff *et al.*, 2010; Skripniková and Řezáčová, 2014; Kunz and Kugel, 2015). A 2×2 contingency table (Wilks, 2006) for radar detections and claims reports was used to compute probability of detection (POD), false alarm rate (FAR) and critical success index (CSI). Whereas POD describes the ability of the algorithms to detect hail correctly, FAR indicates the proportion of wrong detections, i.e. when the algorithm identifies hail over an area but no claims were recorded by the insurance. CSI describes the ability of the detection algorithms of having simultaneously a high POD and a low FAR. A perfect score is represented by a POD and CSI equal to unity and an FAR equal to zero.

Recently Kunz and Kugel (2015) and Skripniková and Řezáčová (2014), for example, validated different hail detection algorithms against loss data provided by building insurance companies using different skill scores and quality measures from categorical verification (Wilks, 2006). They showed that in general radar-based hail information (Waldvogel's method among them) provided a comparatively high probability of detection (POD), but also a high false alarm rate (FAR). Similar results were obtained by Delobbe *et al.* (2005), who verified the POH algorithm with ground reports. However, it is acknowledged that the assessment of the FAR is more complicated compared to the assessment of the POD (e.g. Delobbe *et al.*, 2003; Saltikoff *et al.*, 2010) or not possible at all (e.g. Delobbe and Holleman, 2006). This is due to the fact that if no damage was recorded for a specific area, this does not imply that there was no hail. The reason for any discrepancy might also be that insured losses are controlled by several other factors such as insurance coverage (i.e. the number of insured objects), land use, vulnerability of insured assets (crops, cars or buildings) and insurance regulatory practice. Since the radar usually detects hail at higher altitudes, also melting processes may affect the results. However, since the hailstone's surface is proportional to the square of the radius but the volume is proportional to the cube, melting may influence only small ice particles such as graupel and small hailstones (Mahoney *et al.*, 2012).

4. Results and discussion

Based on the two hail detection algorithms presented in the previous section, different statistics of the estimated hail signals were calculated. The gridded climatological frequency of hail will be discussed first, followed by the monthly distribution, the diurnal cycle and the hail frequency associated with different weather types. Finally, a preliminary validation of the hail products with insurance data is presented. In order to investigate regional differences in the alpine microclimates, hail occurrences are presented with the full radar resolution. We are aware that considering the limited length of the investigation period and the relative rarity of hailstorms, a resolution of 1 km^2 is somewhat high and will reveal details that are partly related to individual events. However, the goal of the study being to present occurrence statistics without making any assumptions about an underlying statistical–physical model of hail, the results are presented in the full resolution of the radar grid.

4.1. Climatological frequency

The seasonal average number of hail days estimated from $\text{POH} > 80\%$ shows several maxima with values between 2 and 4 hail days per km^2 . The most apparent maxima on both sides of the Alps (north and south) are located mainly over the foothills in the pre-alpine region. On the northern parts, enhanced hail frequency is also found over the Jura, the Swabian Jura and Bavarian Alps in Germany. To the south of the Alps, distinct maxima are located along the foothills and in the Po valley (sub-regions 4 and 5 in Figure 1). Over the main chains of the Alps, hail is rare, less than once per year, whereas in other areas the values range between 0.5 and 2.0 days.

The related STD shown in Figure 4 ranges between 0 and 2.8 and correlates in most areas with the mean frequency; areas with higher frequencies show also a high year-to-year variability. Exceptions are found only for the Jura and the Po valley, where the STD is low despite the high frequency of hail. The STDs reflect the well-known high annual variability of hailstorms in general, except for the Jura and the Po valley.

In addition to the POH, the MESHS product was computed over the same period to estimate the frequency of hailstorms including the sizes of the hailstones. Three diameter thresholds of $D = 2, 3$ and 4 cm were considered (Figure 5). Frequency maxima of the MESHS are well related to the distribution of the POH signals presented in Figure 4. For hailstones greater than 2 cm, the frequency maxima reach 1.8 days per season. For larger hailstones, the frequency maxima decrease to 1.4 days (for $D > 3 \text{ cm}$) and

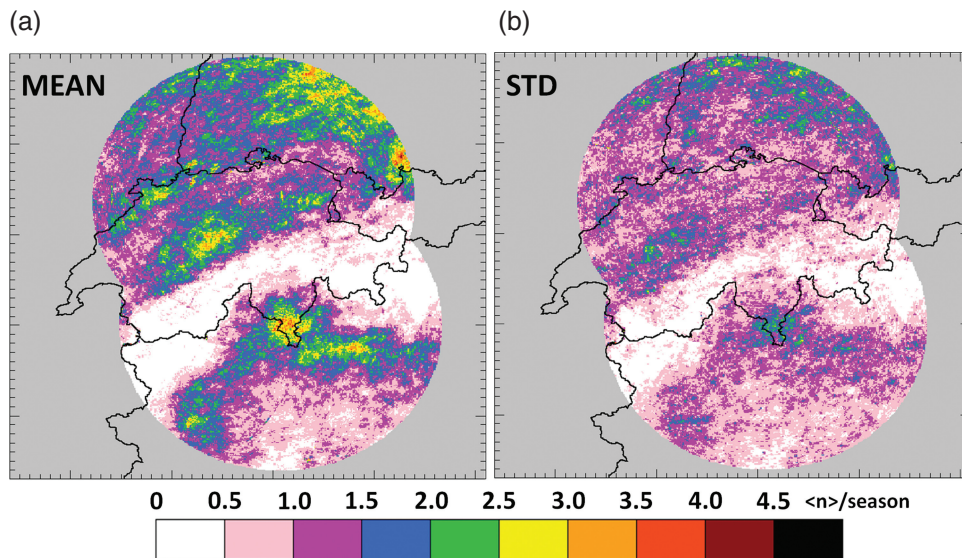


Figure 4. (a) Average number of days with POH > 80% per season (April–September) and per km² during the period 2002–2014 and (b) STD of the number of radar-derived hail days per season.

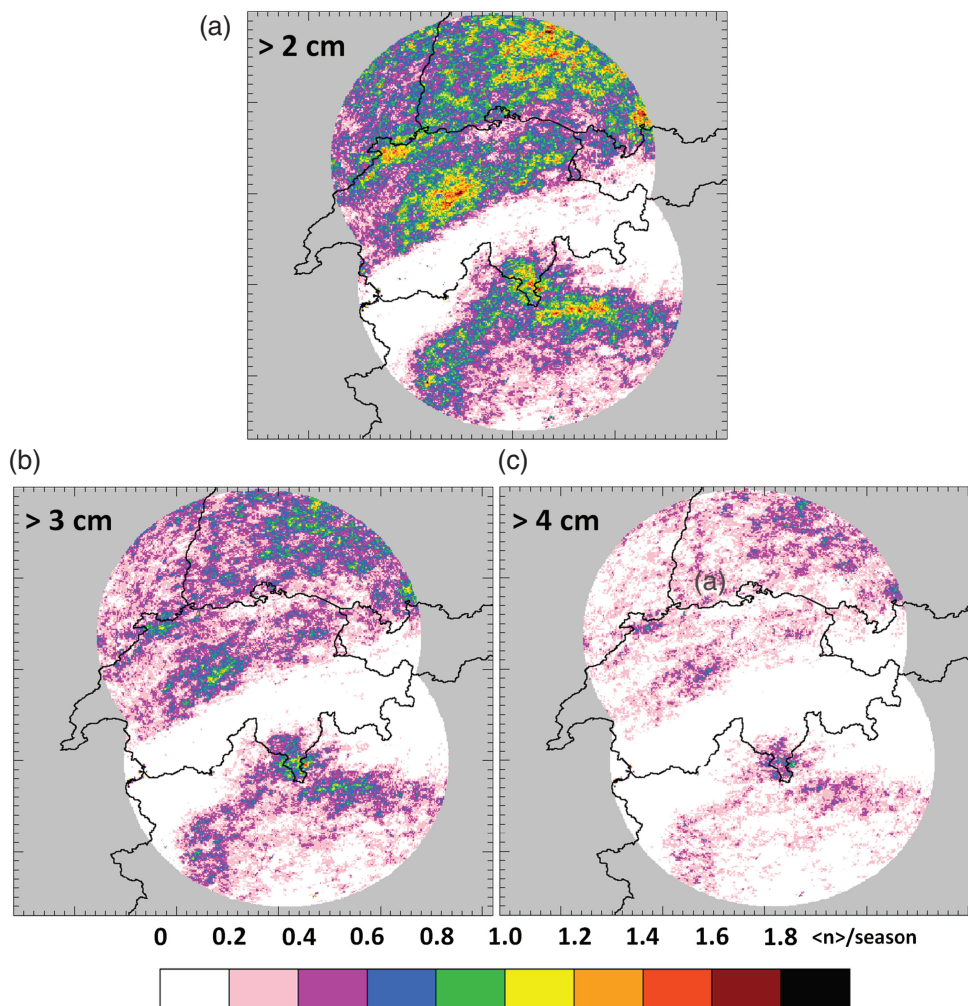


Figure 5. Average number of days with MESHES (a) > 2 cm, (b) > 3 cm and (c) > 4 cm, per season (April–September) and per km² during 2002–2014.

0.6 days per season (for $D > 4$ cm). Due to the high agreement of POH and MESHES ($D > 2$ cm), we consider in the subsequent sections only radar-derived hail days or events estimated when POH > 80%.

Annual mean frequency anomalies were calculated for the whole investigation period and for three different sub-regions: for the entire domain (Figure 6(a)), the northern and the southern pre-alpine and alpine regions (Figure 6(b) and (c)). The displayed hail frequency was accumulated over all pixels of the regions.

Positive (negative) anomalies indicate years where hail was more (less) frequent compared to the multi-year average. In the entire domain, hail frequency is highly variable. STD in northern regions is greater than STD in the south ($STD_{\text{North}} = 1.44 * STD_{\text{South}}$). The years of 2003, 2008 and 2009 show positive anomalies larger than 1 STD, whereas 2013 and 2014 show negative anomalies exceeding -1 STD.

The decrease in hail frequency since 2009 in the entire domain is mainly due to a decrease of hail in the northern alpine area

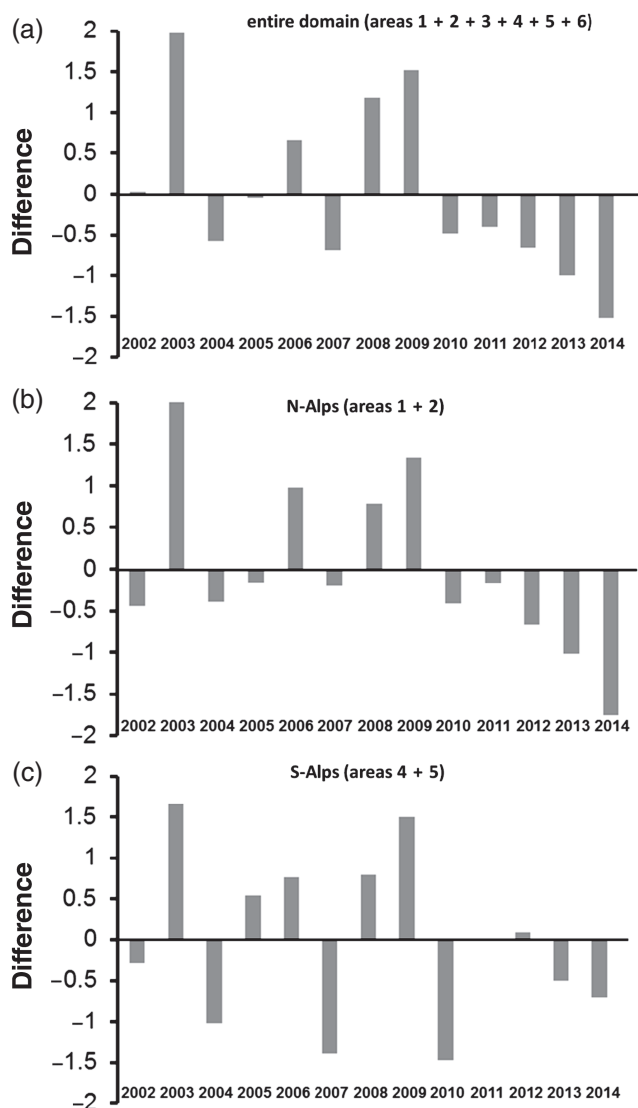


Figure 6. Annual standardized anomalies (POH > 80%) for (a) the entire domain, (b) sub-regions 1 + 2 and (c) sub-regions 4 + 5. See Figure 1 for the location of the sub-regions.

(Figure 6(b)). Four years (2005, 2007, 2010 and 2012) show a strong north-to-south anomaly. These deviations suggest that some of the general weather situations that favour the development of hailstorms in the north are not the same as for the south.

In general, the alpine orography has a direct influence on the distribution of hailstorms; despite of the random nature of hail (Mezher *et al.*, 2012), the identified hot spots suggest that orographic forcing mechanisms and related flow convergence are decisive for hailstorm formation. The repeatability of precipitation events over areas with complex orography has been used to develop nowcasting systems based on past analogues (e.g. Panziera and Germann, 2010). The high spatial variability of hail days together with a maximum over and downstream of hilly terrain (or in its close proximity) as well as the minimum over the highest mountains were also found in other studies performed over regions with complex orography (Changnon and Changnon, 2000; Garcia-Ortega *et al.*, 2007; Počakal *et al.*, 2009; Kunz and Puskeiler, 2010; Berthet *et al.*, 2011, 2013; Cintineo *et al.*, 2012; Eccel *et al.*, 2012; Mezher *et al.*, 2012; Merino *et al.*, 2013). The reduced convective activity over the central chain of the Alps was also found by van Delden (2001) using observations from synoptic weather stations and by Nisi *et al.* (2014) using cloud-to-ground lightning. The triggering and updraught enhancement process is particularly important over the foothills in the vicinity of the Alps or generally over hilly terrain (e.g. Barthlott *et al.*, 2005; Kottmeier *et al.*, 2008; Davolio *et al.*, 2009). In those regions low-level warm and moist air that originates from the plains or from

the Mediterranean south of the Alps is forced to lift due to low-level convergence. These convergence zones are caused by the flow deviations at the hills, by flow-around regimes, or by the outflow of previously developed thunderstorm cells in the alpine valleys. For example, it is well known that the Po valley and the southern Pre-alpine region are dominated by anabatic–katabatic wind systems (Morgan, 1973; Gladich *et al.*, 2011). For these reasons, the foothills of the alpine chain represent one of the regions in Europe with the most frequent convection initiation (Collier and Lilley, 1994; Huntrieser *et al.*, 1996; van Delden, 2001).

4.2. Monthly distribution

The radar-derived hail frequency shows a pronounced seasonal cycle with a maximum in June/July (Figure 7). In April and September, hailstorms are quite rare and occur without distinct spatial patterns. From October to March, hailstorms are extremely rare (only five cases were observed during the last 13 years). In these months, the air masses are usually unfavourable for severe convection due to the low magnitude of the lapse rate. In May, hail frequency increases slightly both in the northern part of the Alps and in southern Germany, whereas in June it increases more or less over the whole domain. Due to more unstable conditions in the mean, not only pre-frontal and frontal embedded storms with high wind shear conditions, but also stationary air-mass convection are capable of producing hail in June. The highest hail frequency can be found over the Jura and the alpine foothills in the Po valley.

The month of July is the most active month with the maximum frequency on both sides of the Alps with values of about 1.8 hail days. Most pronounced are the maxima in the vicinity of the Alps, i.e. on the northern and southern sides. Over the Jura and in southwest Germany, however, hail frequency is reduced compared to June. This suggests again that the Alps play an important role for the initiation of severe convective storms over the foothills. In August, hail frequency is lower in the entire domain. The decrease is particularly evident north of the Alps, but less in the south, where warm and moist condition due to the presence of the Mediterranean Sea still provide favourable conditions for the development of severe storms. Similar results were found in Griffith (1972). The strong decrease in hail activity in August is also confirmed by the monthly distribution of insurance claim reports (Figure 8).

Other studies for Switzerland (Admirat *et al.*, 1985) found a maximum in hail occurrence between mid-June and mid-July, which is close to our results. Investigations for adjacent regions like north-eastern Italy (Giaiotti *et al.*, 2003), the continental part of Croatia (Počakal *et al.*, 2009) or the Czech Republic (Skripniková and Řezáčová, 2014) identified the hail maximum during June or July (southwest Germany (Mohr, 2013)). Furthermore, in France, Fraile *et al.* (2003) and Berthet *et al.* (2011) found a bimodal distribution, with an absolute maximum in May and a secondary one in July. All climatologies over central Europe are consistent showing the minimum in hail occurrence in autumn, in winter and early in the spring. If the air-mass conditions required for sustaining severe convection, i.e. high instability and wind shear conditions, are not met, storms are often short-lived single cells with a limited vertical development and without a well-structured hail core. Because of relatively low temperatures and the reduced effect of melting, graupel showers are common especially early in the spring. This is often observed in the northern part of the Alps, but also in other regions. The presence of cold air masses and the increased frequency of graupel showers have already been hypothesized by Mezher *et al.* (2012).

4.3. Diurnal cycle

Hourly radar-derived hail frequency for the entire domain and for the six sub-regions features a distinct diurnal cycle during all months and regions with a maximum in the late afternoon and

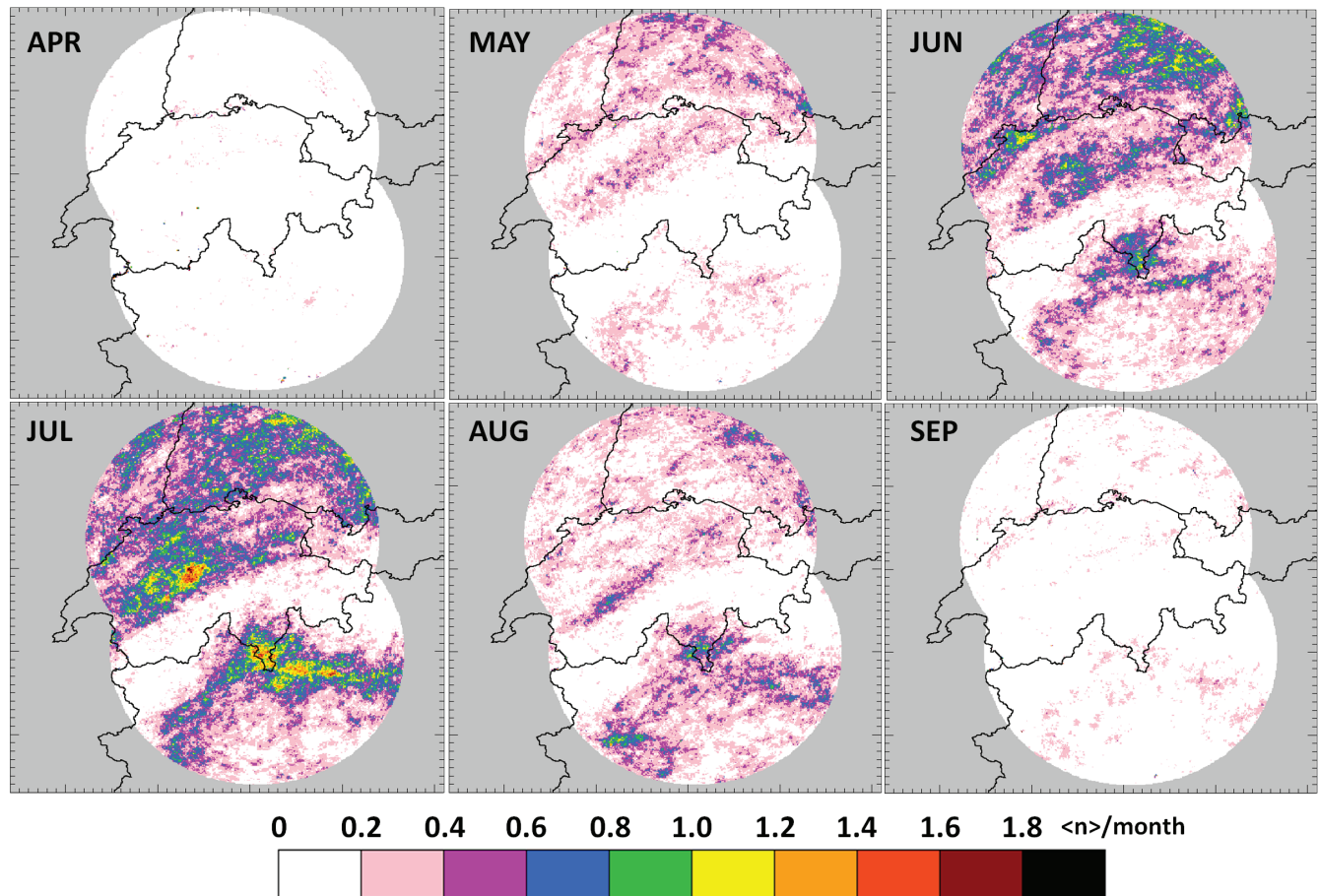


Figure 7. Average number of radar-derived hail days (POH > 80%) for each month (April–September) and km² during 2002–2014.

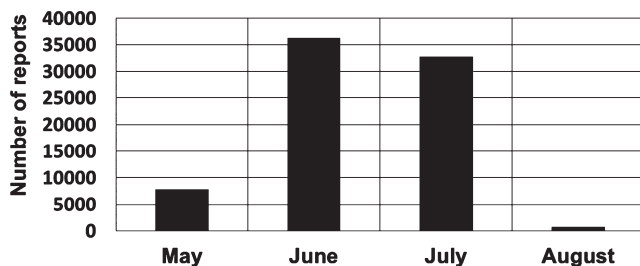


Figure 8. Total number of claims per month for the period 2003–2012.

a minimum in the morning hours (Figure 9). Most hail events occur in the afternoon hours between 1300 and 1800 UTC (i.e. approximately 1100 and 1600 local time), whereas a minimum is evident in the early morning. From May to July, the three months when hail is more frequent, the diurnal cycle peaks slightly later south of the Alps compared to the northern sub-regions. For example, over the northern Pre-alps the peak is between 1500 and 1700 UTC, whereas it is two hours later over the southern Pre-alps.

In the south, late afternoon–evening storms are relatively frequent during summer months. Mesoscale descent of cold air from the Alps and thunderstorm outflows may trigger convective cells in the Pre-alpine area (Morgan, 1973). Gladich *et al.* (2011) found that the evening changes in the diurnal wind regimes can produce flow convergences that may trigger or invigorate convective cells. Furthermore, Giaiotti *et al.* (2003) found that a greater amount of water vapour from July to September is the reason for an increased evening hailstorm occurrence over Friuli Venezia Giulia in the northeastern part of Italy. Secondary maxima at night were also found over southwestern France by Dessens (1986).

Some sub-regions show larger variability in some months (e.g. the Jura in August). This is a consequence of the small number

of hailstorms involved. In these cases, relative maxima are not statistically representative. The spatial distribution of the two-hour periods (UTC), when on average the highest hail frequency has been recorded, shows several larger and almost homogeneous areas (Figure 10), but also sharp gradients reflecting the partly stochastic nature of deep moist convection.

The Swabian Jura and the Jura mountains in the western part of Switzerland show the earliest hail peaks (1000–1400 UTC). Differential heating, orographic triggering and local low-level convergence may explain the early convection initiation over these regions (e.g. Kottmeier *et al.*, 2008). Another possible explanation is the triggering of hailstorms by pre-frontal uplift (Schemm *et al.*, 2016). Since most of the fronts enter the investigation area from the west, related convection must develop earlier in those areas. Outflow boundaries of the early convective development over the Jura mountains may act as an additional triggering mechanism for the subsequent formation of convective cells over the western regions, where the peaks are between 1200 and 1600 UTC. These cells usually move towards the east during the afternoon, affecting the central part of the northern pre-alpine region (Lucerne–Zürich) in the late afternoon with peaks between 1600 and 2000 UTC. These mechanisms may explain the pronounced west-to-east gradient visible in Figure 10 in the northern part of the Alps.

In the southern pre-alpine area, a larger spatial variability of the hail peak hour is found compared to the northern parts. Over the same region, an interesting line of hail signal peaks late in the night (pink-violet colours corresponding to 0200–0600 UTC) is visible along the southern border of the pre-alpine foothills (right part of the investigation sub-region 4). This nighttime convective development may be explained by low-level convergence produced by katabatic wind systems (Morgan, 1973; Gladich *et al.*, 2011).

In the Po valley a large, almost homogeneous area with a peak frequency between 1800 and 2200 UTC is evident. Over

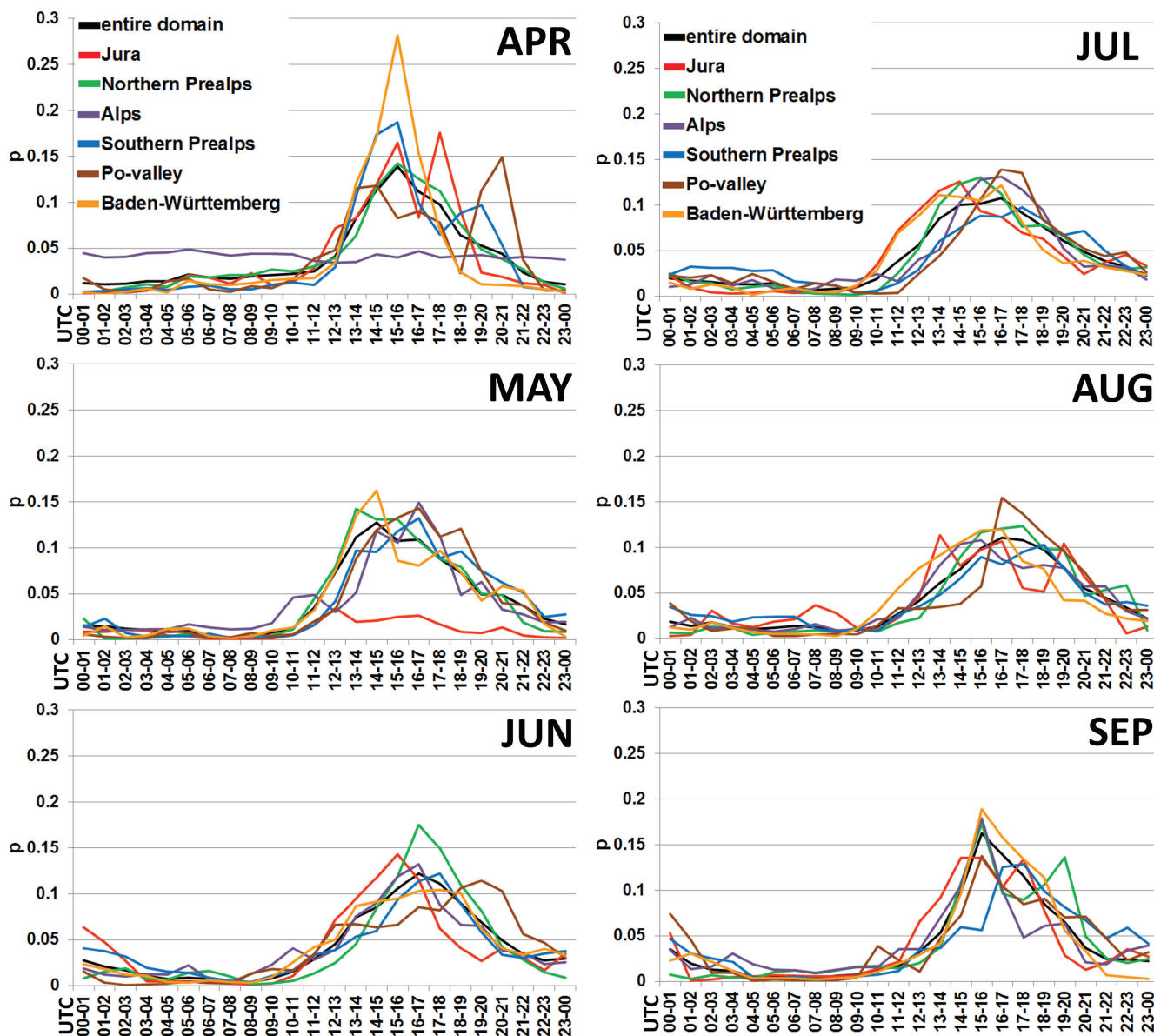


Figure 9. Hourly radar-derived hail frequency (normalized) for the entire domain and six sub-regions. The diagrams show the diurnal cycle of hail days between 0000 and 2400 UTC for the period April–September and 2002–2014. A hail hour is defined as the hour when a POH value above 80% is detected in the region.

flat areas, the absence of important triggering mechanisms such as differential heating or orographic uplift may delay convection initiation and, consequently, the formation of severe storms.

4.4. Hail occurrence and weather types

Typical circulation patterns are investigated using large-scale weather types (WT) provided by MeteoSwiss (Weusthoff, 2011). A ten-class WT classification based on geopotential and wind direction at 500 hPa was used here. Since the frequency of the different WTs is not homogeneous, the results were normalized by the number of days for each weather type. WT1, WT2 and WT8, which correspond to westerly, southwesterly and southerly flow, are the most frequent WTs. Highest hail frequency is found during the southwesterly flow regime (WT2), with maximum frequency values of about 5% per grid point (Figure 11). Similar hail-favouring WTs were identified in several other studies for other areas in central and southern Europe (e.g. Bider, 1954; Willemse, 1995; Hohl and Schiesser, 2001; Kunz and Sander, 2009; Kunz and Puskeiler, 2010; Berthet *et al.*, 2013; Merino *et al.*, 2013). Days characterized by westerly flow (WT1) are less favourable for hail. During southerly flow (WT8), higher frequency in hail occurrence is found over the Bavarian Alps. Note, however, that the latter maximum is found at a large distance from the Albi radar location, thus the results may be not reliable.

For the types WT5, WT4 and WT3, namely northeasterly, northerly and northwesterly flow over central Europe, radar-derived hail signals occur less frequently over the entire domain. However, some localized maxima are also present in the southern Pre-alps for WT4 and WT5.

4.5. Verification of radar-based hail algorithms with insurance data

Since radar-based hail detection algorithms are based on proxy data, verification with ground observations is required. Since no direct hail measurements are available for the investigation area, a preliminary assessment of the POH and MESHS skills uses loss data from an automobile insurance company. Compared to buildings, cars have the advantage of a higher vulnerability; however, they have the disadvantage of being mobile, and insurance loss data may be affected by this additional source of uncertainty. Further, this dataset does not allow us to perform verifications over areas with very low population density, or evaluate non-severe storms with hailstone sizes <2 cm.

Overall the superposition of the insurance claim reports with daily maximum POH values shows a good agreement (Figure 12 an example for 23 July 2009). Only over mountainous areas or less urbanized regions, where few roads exist, is the agreement low.

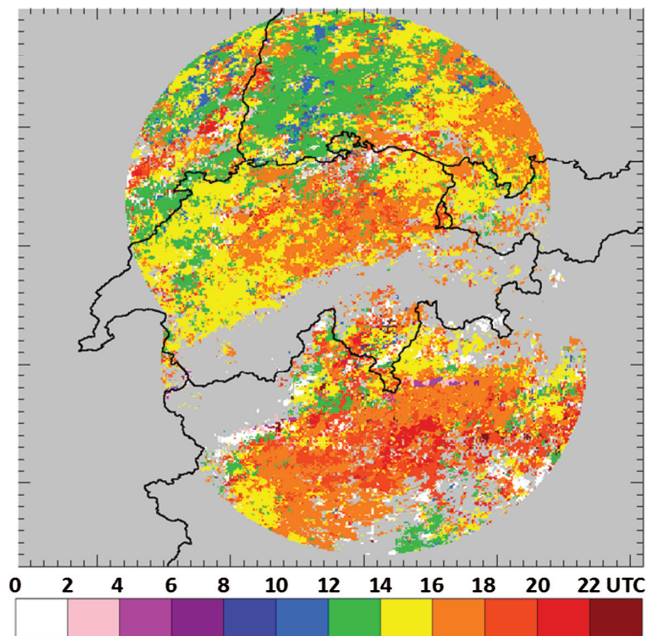


Figure 10. Time (hour UTC) of the highest radar-derived hail frequency per km² for the period April–September, 2002–2014. Only pixels affected by at least three hailstorms with POH > 80% were considered.

We therefore performed a quantitative verification only over areas where the presence of cars is highly probable, namely the 25 most populated urban areas in Switzerland (Figure 13). For the verification, more than 200 days have been selected; for each of these days the POH, the MESHS and/or insurance claim reports (≥ 10 per urban area) indicated that there was hail over at least one of these areas.

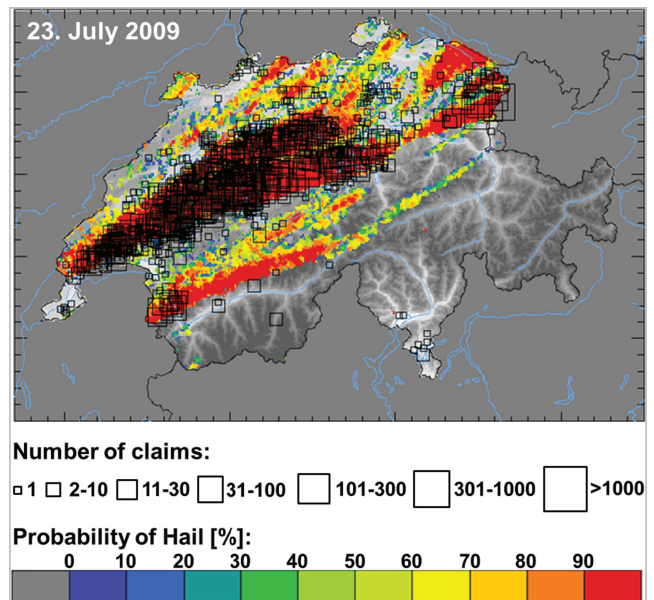


Figure 12. POH daily maximum (colour shading) and number of car claims per postal code zone (black squares) on 23 July 2009.

The purpose of the preliminary verification is to investigate how well the different POH and MESHS thresholds relate to the occurrence of damage to automobiles. For this, the 90th percentiles among the POH or MESHS values distribution of the considered area have been used. It would be interesting to validate the hailstone dimensions provided by MESHS, but unfortunately in the insurance dataset this information is not available.

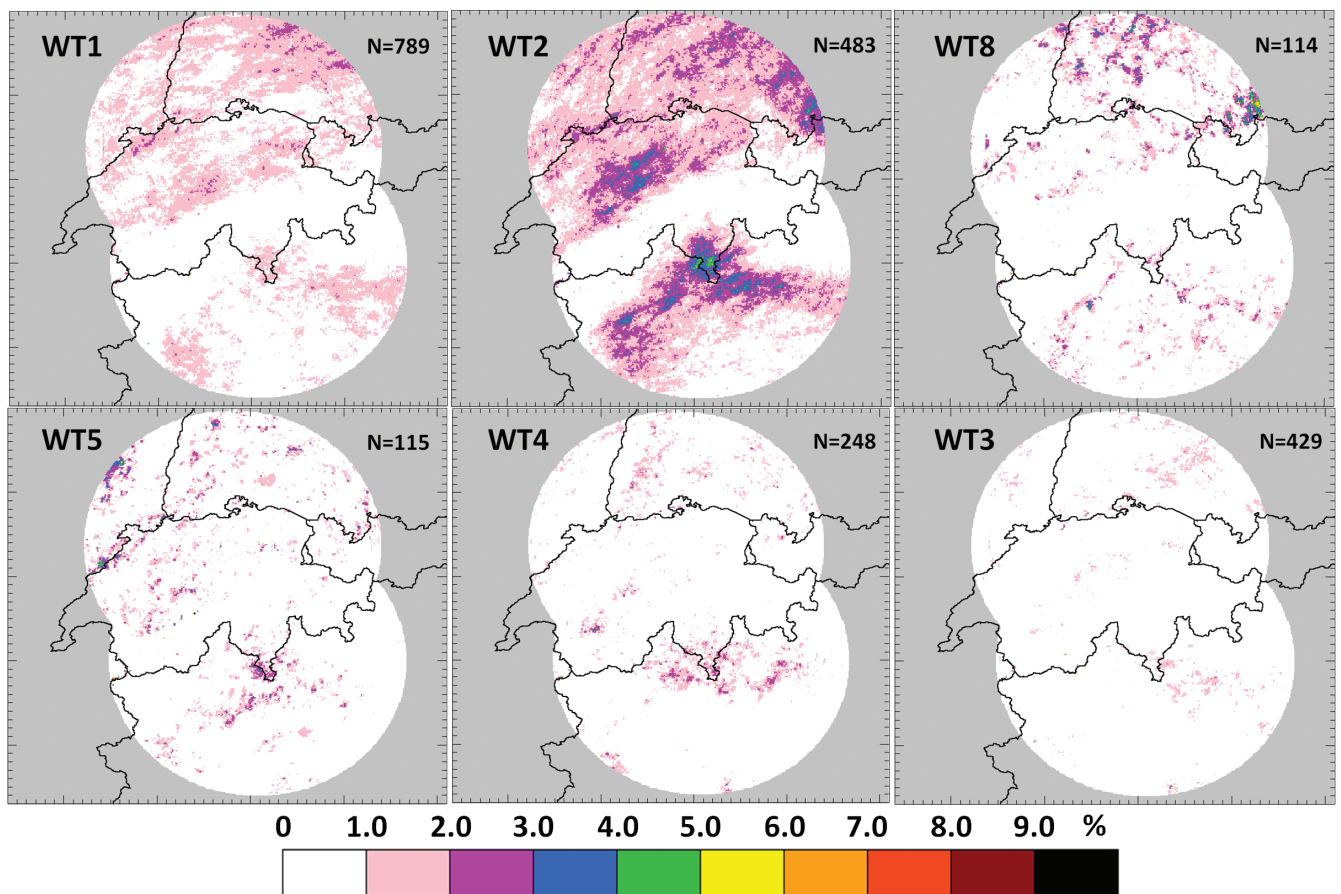


Figure 11. Normalized frequency of radar-derived hail days, i.e. days with POH > 80%, for different weather types for the period April–September, 2002–2014. N is the number of days in each class. Only the six weather types which show a hail frequency in excess of 1% are shown: westerly flow (WT1); southwesterly flow (WT2); southerly flow (WT8); northeasterly flow (WT5); northerly flow (WT4); northwesterly flow (WT3); cf. Table 2.

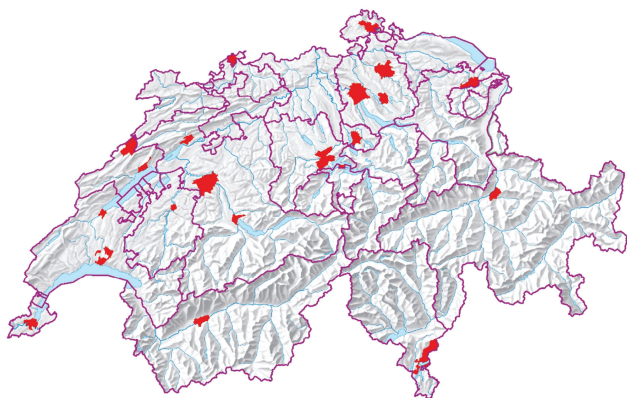


Figure 13. The 25 most populated urban areas in Switzerland (red areas) selected for the verification of the radar-based hail identification. The following agglomerations have been considered: Zürich, Geneva, Basel, Lausanne, Bern, Winterthur, Lucerne, St Gallen, Lugano, Biel, Thun, Köniz, La Chaux-de-Fonds, Freiburg, Schaffhausen, Chur, Vernier, Neuchâtel, Uster, Sitten, Lancy, Emmen, Yverdon-les-Bains, Zug and Kriens.

Figure 14 shows three skill scores for different POH and MESHS thresholds. Overall, a high POD (in this study $\text{POD} \geq 0.84$) is found for all POH thresholds (Figure 14(a)). On the other hand, the FAR is also high (≥ 0.7 for $\text{POH} \leq 70\%$). An evident decrease of the FAR is visible for increasing POH thresholds (0.54 for $\text{POH} = 80\%$ and 0.49 for $\text{POH} \geq 90$). A similar behaviour of the FAR was observed by other authors, for example Aran *et al.* (2007) or Kessinger *et al.* (1995). This is an indication that damage due to hail increases significantly with POH values greater than 70–80%. A further confirmation is provided by Saltikoff *et al.* (2010) and Delobbe *et al.* (2005), who showed that in Belgium and the Netherlands all events with hailstones larger than 2 cm corresponded to a POH of at least 80%. According to the findings of Saltikoff *et al.* (2010) and Delobbe *et al.* (2005), it can be expected that the FAR for lower POH values will decrease if the radar hail detections are validated against crop damage, which occurs for small hail already. In Switzerland, first results from a pilot study employing automatic hail detectors (Löffler-Mang *et al.*, 2011) showed that soft hail or even graupel are often detected for lower POH values (i.e. 20–50%). The values of the CSI are in the range of other studies, e.g. by Holleman (2001) or Kunz and Kugel (2015). CSI values in excess of 0.4 for $\text{POH} > 80\%$ confirm the plausibility of this threshold considered in our study.

Skill scores for the MESHS (Figure 14(b)) show slightly lower PODs (≥ 0.74), but much lower FARs (≤ 0.53). On the one hand, it can be expected that higher MESHS values result in a higher POD (i.e. increased connection to damage to automobiles). On the other hand, the population of MESHS classes is not equally distributed (few cases of MESHS-60 mm compared to the number of MESHS-20 mm cases). Therefore the POD does not increase linearly with increasing MESHS thresholds. Because of small

populations, the skill scores for MESHS values greater than 40 mm should be taken with care.

The validation based on insurance loss data is challenging and the results have to be analysed carefully. Kunz and Kugel (2015) discuss several reasons for the high FARs. First, the POH algorithm was originally developed by comparing radar observations with hailpad data, which are able to detect smaller hailstones. Therefore, high POH values (i.e. $> 70\%$) can be reached even if no damaging hailstones for cars, i.e. hailstones ≥ 2 cm, are present. Furthermore, the spatial resolution and errors of both datasets may influence the skill scores considerably. For example, in the case of strong winds, hailstone drift represents an error source for the radar data (Schuster *et al.*, 2006). Concerning insurance claim reports, uncertainties in the spatial and temporal allocation of the damage and uncertainty in the presence of cars (population density, insurance contract distributions) are main error sources. Since for our investigation domain no other hail observations exist, insurance claim reports represent the best available verification data for hail.

5. Summary and conclusions

A 13-year hail assessment has been conducted by reprocessing and homogenizing volumetric radar data (from April to September) over Switzerland and adjacent countries. Radar-based hail detection algorithms have been used to investigate the spatial distribution and frequency of hail signals with a high spatio-temporal resolution. Indirect hail observations based on radar reflectivity and melting height as proxy data are valuable especially in areas where no ground observations are available, like the area considered in this study.

The results in terms of radar-derived hail days during the 13-year period are located along the foothills of the Alps in the northern and southern pre-alpine region, over northwestern Switzerland, the Jura as well as over southern Germany and the Bavarian Alps. Maximum values range between 2 and more than 4 hail days per summer season. It has been found that the variability in hail occurrence in the north is greater compared to the south (144% of the STD).

Monthly radar-derived hail maps show a distinct seasonal cycle with the maximum for June and July. During May and August differences in the hail frequency are found for areas north and south of the Alps. During late spring, hailstorm activity is more pronounced in the north, whereas in late summer, hail is more frequent in the south, especially over the Po valley, where the Mediterranean Sea still provides the warm and moist air favourable for the development of hailstorms.

An evident diurnal cycle is found for all six sub-regions from April to September. Clear spatial differences in the time of the day, when hail is most frequent, are found. Hail occurs earlier in the day in the western part of Switzerland and in the Swabian Jura. In the northern pre-alpine area a clear west-to-east gradient is visible,

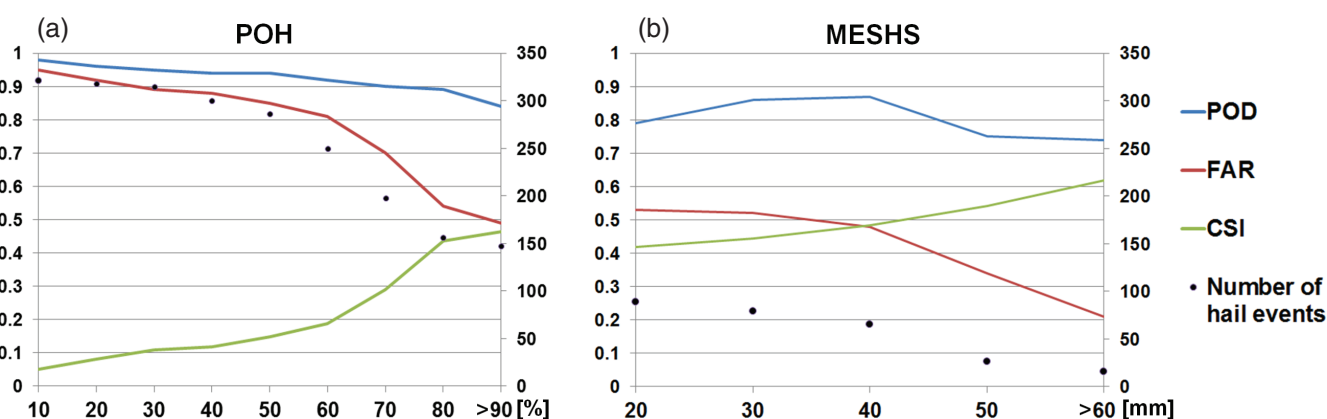


Figure 14. Comparison of three skill scores (POD, FAR and CSI, left axis) and number of hail events (right axis) detected with different (a) POH and (b) MESHS thresholds. The verification is performed against car insurance reports over 25 selected urban areas between 2003 and 2012.

whereas in the southern pre-alpine area hail tends to occur later in the day. However, in these areas a larger variability is found.

Several weather types are favourable for hail formation. Considering wind direction at 500 hPa, hail occurs most frequently with southwesterly flow regimes. For both sides of the Alps the second most hail-producing wind regime is represented by the westerly flow. In this case, hail occurrences and distributions are strongly reduced, especially in the southern areas.

However, the results show that hail can also occur on a more local scale during southerly, northeasterly, northerly and northwesterly flow regimes.

The two considered radar-based hail detection algorithms were validated with motor loss data from an insurance company. The results show that both POH and MESHS are reliable proxies for hail detection, yielding a POD higher than 75%. Several uncertainties related to the insurance claim reports result in a high FAR, especially for low POH values. However, for POH values greater than 80%, which is used in this study, the FAR decreases rapidly to almost 50%. Despite a slight overestimation of radar-derived hail occurrence against insurance claim reports, it can be concluded that the hail distributions presented in this work are fairly robust and reliable.

The challenges in using radar-based approaches over complex terrain have been described previously, showing that several effects can affect the radar measurements. However, most of them do not or only marginally affect the radar products used in this study. The fact that two or more hail events can affect the same area in one day results in a slight underestimation of the number of hail events since monthly and yearly distributions are based on daily hail maxima. However, over the considered period 0.02% of the area has been affected by two hailstorms (POH > 80%) in one day. By using MESHS or reducing the time aggregation (hourly composites) this issue is even less important. The two empirical algorithms (POH, MESHS) used in this study are based on the idea that strong radar reflectivities are mainly caused by large hydrometeors. The POH has been verified and used operationally for several years, providing reliable results (e.g. Delobbe *et al.*, 2005; Saltikoff *et al.*, 2010; Skripniková and Řežáčová, 2014; Kunz and Kugel, 2015) and independent verifications with insurance data are presented in section 4.5. Because of the scarcity of hail size observations over Switzerland in the past, further effort for the verification of the MESHS is needed in the near future. Next steps include its verification by means of data collected with (i) the new automatic hail-sensors network in Switzerland (Löffler-Mang *et al.*, 2011) and (ii) hail crowd-sourcing data (e.g. Elmore *et al.*, 2014).

Furthermore, an object-based analysis of hailstorm characteristics and their environmental conditions over Switzerland is going to be performed using a radar-based thunderstorm tracking algorithm (Hering *et al.*, 2008). The overall goal is to investigate the conditions and the characteristics which lead to the formation and intensification of hailstorms. Expected findings will be potentially interesting for thunderstorm nowcasting purposes.

Acknowledgements

The authors thank M. Boscacci and L. Clementi (MeteoSwiss) for technical support, P. Ambrosetti, S. Zanini (MeteoSwiss), A. Martynov and A. Zischg (University of Bern) and S. Schemm (University of Bergen) for scientific discussions as well as for providing support in the review of the scientific documentation. We kindly thank M. Künzler and L. Thomi (Die Mobiliar) for providing insurance loss data and related support and S. Morel (University of Bern) for the preparation and preliminary analysis of the insurance claim report dataset and S. Nisi for the graphic design.

References

Admirat P, Goyer GG, Wojtjw L, Carte EA, Roos D, Lozowski E. 1985. A comparative study of hailstorms in Switzerland, Canada and South Africa. *J. Clim.* **5**: 35–51.

- Amburn SA, Wolf PL. 1997. VIL density as a hail indicator. *Weather and Forecasting* **12**: 473–478.
- Aran M, Sairouni A, Bech J, Toda J, Rigo T, Cunillera J, Moré J. 2007. Pilot project for intensive surveillance of hail events in Terres de Ponent (Lleida). *Atmos. Res.* **83**: 315–335.
- Barthlott C, Corsmeier C, Meißner C, Braun F, Kottmeier C. 2005. The influence of mesoscale circulation systems on triggering convective cells over complex terrain. *Atmos. Res.* **81**: 150–175.
- Basara JB, Cheresnick DR, Mitchell D, Illston BG. 2007. An analysis of severe hail swaths in the Southern Plains of the United States. *Trans. GIS* **11**: 531–554.
- Berthet C, Dessens J, Sánchez JL. 2011. Regional and yearly variations of hail frequency and intensity in France. *Atmos. Res.* **100**: 391–400.
- Berthet C, Wesolek E, Dessens J, Sánchez JL. 2013. Extreme hail day climatology in southwestern France. *Atmos. Res.* **123**: 139–150.
- Betschart M, Hering A. 2012. Automatic hail detection at MeteoSwiss. *Arbeitsberichte der MeteoSchweiz* **238**: 61. <http://www.meteoschweiz.admin.ch/content/dam/meteoswiss/en/Ungebundene-Seiten/Publikationen/Fachberichte/doc/ab238.pdf> (accessed 01 September 2015).
- Bider M. 1954. Statistische Untersuchungen über die Hagelhäufigkeit in der Schweiz und ihre Beziehungen zur Großwetterlage. *Arch. Meteorol. Geophys. Bioklim.* **6**: 66–90 (In German).
- Bryan GH, Wyngaard JC, Fritsch JM. 2003. Resolution requirements for the simulation of deep moist convection. *Mon. Weather Rev.* **131**: 2394–2416.
- Changnon SA. 1978. The climatology of hail in the United States. Hail: A review of hail science and hail suppression. *Meteorol. Monogr. Am. Meteorol. Soc.* **38**: 107–128.
- Changnon SA, Changnon D. 2000. Long-term fluctuations in hail incidences in the United States. *J. Clim.* **13**: 658–664.
- Changnon D, Changnon SA, Changnon SS. 2001. A method for estimating crop losses from hail in uninsured periods and regions. *J. Appl. Meteorol.* **40**: 84–91.
- Cintineo JL, Smith TM, Lakshmanan V, Brooks HE, Ortega KL. 2012. An objective high resolution hail climatology of the contiguous United States. *Weather and Forecasting* **27**: 1235–1248.
- Collier CG, Lilley RBE. 1994. Forecasting thunderstorm initiation in north-west Europe using thermodynamic indices, satellite and radar data. *Meteorol. Appl.* **1**: 74–84.
- Davolio S, Buzzi A, Malguzzi P. 2009. Orographic triggering of long lived convection in three dimensions. *Meteorol. Atmos. Phys.* **103**: 35–44.
- Dee DP, Uppala SM, Simmons AJ, Berrisford P, Poli P, Kobayashi S, Andrae U, Balmaseda MA, Balsamo G, Bauer P, Bechtold P, Beljaars ACM, van de Berg L, Bidlot J, Bormann N, Delsol C, Dragani R, Fuentes M, Geer AJ, Haimberger L, Healy SB, Hersbach H, Hólm EV, Isaksen I, Kållberg P, Köhler M, Matricardi M, McNally AP, Monge-Sanz BM, Morcrette J-J, Park B-K, Peubey C, de Rosnay P, Tavolato C, Thépaut J-N, Vitart F. 2011. The ERA-Interim reanalysis: Configuration and performance of the data assimilation system. *Q. J. R. Meteorol. Soc.* **137**: 553–597, doi: 10.1002/qj.828.
- van Delden A. 2001. The synoptic setting of thunderstorms in western Europe. *Atmos. Res.* **56**: 89–110.
- Delobbe L, Holleman I. 2006. Uncertainties in radar echo top heights used for hail detection. *Meteorol. Appl.* **13**: 361–374.
- Delobbe L, Dehenaux D, Hamid K, Neméghaire J. 2003. 'Hail detection using radar observations: case studies in the summer 2002.' Scientific and Technical Publication, Royal Meteorological Institute of Belgium, Nr. 029.
- Delobbe L, Holleman I, Dehenaux D, Neméghaire J. 2005. 'Verification of radar-based hail detection products.' In *Proceedings of the WWRP Symposium on Nowcasting and Very Short Range Forecasting (WSN05)*, 5–9 September 2005. Toulouse, France.
- Dessens J. 1986. Hail in southwestern France. I: Hailfall characteristics and hailstorm environment. *J. Clim. Appl. Meteorol.* **25**: 35–47.
- Dessens J, Fraile R. 1994. Hailstone size distributions in southwestern France. *Atmos. Res.* **33**: 57–73.
- Dessens J, Fraile R, Pont V, Sánchez JL. 2001. Day-of-the-week variability of hail in southwestern France. *Atmos. Res.* **59–60**: 63–76.
- Dessens J, Berthet C, Sánchez JL. 2009. 'Yearly fluctuation of hail precipitation in France.' In *Proceedings of 5th European Conference on Severe Storms*, 12–16 October. Landshut, Germany.
- Dixon M, Wiener G. 1993. TITAN: Thunderstorm Identification, Tracking, Analysis, and Nowcasting – a radar-based methodology. *J. Atmos. Oceanic Technol.* **10**: 785–797.
- Donaldson R. 1961. Radar reflectivity profiles in thunderstorms. *J. Meteorol.* **18**: 292–305.
- Douglas RH. 1963. Recent hail research: A review. *Meteorol. Monogr.* **5**: 157–172.
- Eccel E, Ferrari P. 1997. 'La grandine in Trentino: risultati dell'analisi climatologica per il ventennio 1974–1993.' Istituto Agrario di San Michele, Quaderni di Esperienze & Ricerche n. 3 (In Italian).
- Eccel E, Cau P, Riemann-Campe K, Biasoli F. 2012. Quantitative hail monitoring in an alpine area: 35-year climatology and links with atmospheric variables. *Int. J. Climatol.* **32**: 503–517.
- Edwards R, Thompson RL. 1998. Nationwide comparisons of hail size with WSR-88D vertically integrated liquid water and derived thermodynamic sounding data. *Weather and Forecasting* **13**: 277–285.

- Elmore KL, Flamig ZL, Lakshmanan V, Kaney BT, Farmer V, Reeves HD, Rothfusz LP. 2014. mPING: Crowd-sourcing weather reports for research. *Bull. Am. Meteorol. Soc.* **95**: 1335–1342, doi: 10.1175/BAMS-D-13-00014.1.
- Footo GB, Knight CA. 1979. Results of a randomized hail suppression experiment in northeast Colorado. Part I: Design and conduct of the experiment. *J. Appl. Meteorol.* **18**: 1526–1537.
- Footo GB, Krauss TW, Makitov V. 2005. Hail metrics using convectional radar. In *Proceedings of 16th Conference on Planned and Inadvertent Weather Modification*, 10–13 January 2005. San Diego, CA: 1–6. American Meteorological Society: Boston.
- Foresti L, Kanevski M, Pozdnoukhov A. 2011. Data-driven exploration of orographic enhancement of precipitation. *Adv. Sci. Res.* **6**: 129–135.
- Frailé R, Berthet C, Dessens J, Sánchez JL. 2003. Return periods of severe hailfalls computed from hailpad data. *Atmos. Res.* **67–68**: 189–202.
- García-Ortega E, Fita L, Romero R, Lopez L, Ramis C, Sánchez JL. 2007. Numerical simulation and sensitivity study of a severe hailstorm in northeast Spain. *Atmos. Res.* **85**: 225–241.
- Germann U. 1999. Radome attenuation – a serious limiting factor for quantitative radar measurements? *Meteorol. Z.* **8**: 85–90.
- Germann U, Galli G, Boscacci M, Bolliger M. 2006. Radar precipitation measurement in a mountainous region. *Q. J. R. Meteorol. Soc.* **132**: 1669–1692.
- Germann U, Boscacci M, Gabella M, Sartori M. 2015. Radar design for prediction in the Swiss Alps. *Meteorol. Techn. Int.* **4**: 42–45.
- Giaiotti D, Nordio S, Stel F. 2003. The climatology of hail in the plain of Friuli Venezia Giulia. *Atmos. Res.* **67–68**: 247–259.
- Gladich I, Gallai I, Giaiotti DB, Stel F. 2011. On the diurnal cycle of deep moist convection in the southern side of the Alps analysed through cloud-to-ground lightning activity. *Atmos. Res.* **100**: 371–376.
- Griffith MM Jr. 1972. A general description of the hail problem in the Po valley of northern Italy. *J. Appl. Meteorol.* **12**: 338–353.
- Held G. 1978. The probability of hail in relation to radar echo heights on the South African Highveld. *J. Appl. Meteorol.* **17**: 755–762.
- Hering AM, Morel C, Galli G, Sénési S, Ambrosetti P, Boscacci M. 2004. Nowcasting thunderstorms in the Alpine region using a radar based adaptive thresholding scheme. In *Proceedings of 3rd European Conference Radar in Meteorology and Hydrology (ERAD)*, 6–10 September 2004. Visby, Sweden: 1–6. Copernicus: Göttingen, Germany.
- Hering AM, Germann U, Boscacci M, Sénési S. 2008. Operational nowcasting of thunderstorms in the Alps during MAP D-PHASE. In *Proceedings of 5th European Conference on Radar in Meteorology and Hydrology (ERAD)*, 30 June–4 July 2008. Helsinki: 1–5. Copernicus: Göttingen, Germany.
- Hohl R, Schiesser HH. 2001. Cloud-to-ground lightning activity in relation to the radar-derived hail kinetic energy in Switzerland. *Atmos. Res.* **56**: 375–396.
- Hohl R, Schiesser HH, Knepper I. 2002. The use of weather radars to estimate hail damage to automobiles: An exploratory study in Switzerland. *Atmos. Res.* **61**: 215–238.
- Holleman I. 2001. 'Hail detection using single-polarization radar.' KNMI publication WR-2001-01. http://www.knmi.nl/publications/fulltexts/wr_hail.pdf (accessed 01 September 2015).
- Houze RA Jr, Schmid W, Fovell RG, Schiesser HH. 1993. Hailstorms in Switzerland: Left movers, right movers and false hooks. *Mon. Weather Rev.* **121**: 3345–3370.
- Huntresser H, Schiesser HH, Schmidt W, Waldvogel A. 1996. Comparison of traditional and newly developed thunderstorm indices for Switzerland. *Weather and Forecasting* **12**: 108–125.
- Joe P, Burgess D, Potts R, Keenan T, Stumpf G, Treloar A. 2004. The S2K severe weather detection algorithms and their performance. *Weather and Forecasting* **19**: 43–63.
- Johnson JT, MacKeen PL, Witt A, Mitchell ED, Stumpf GJ, Eilts MD, Thomas KW. 1998. The Storm Cell Identification and Tracking (SCIT) algorithm: An enhanced WSR-88D algorithm. *Weather and Forecasting* **13**: 263–276.
- Joss J, Schaedler B, Galli G, Cavalli R, Boscacci M, Held E, Della Bruna G, Kapfenberger G, Nespor V, Spiess R. 1998. *Operational Use of Radar for Precipitation Measurements in Switzerland*. vdf Hochschulverlag AG. ETH Zürich. http://www.meteoschweiz.admin.ch/content/dam/meteoswiss/fr/Mess-und-Prognosesysteme/doc/meteoswiss_operational_use_of_radar.pdf (accessed 02 December 2015); Zürich, Switzerland.
- Kessinger CJ, Brandes EA, Smith JW. 1995. A comparison of the NEXRAD and NSSL hail detection algorithms. In *Preprints of 27th Conference on Radar Meteorology*. Vail, Colorado: 603–605. American Meteorological Society: Boston.
- Kottmeier C, Kalthoff N, Bathlott C, Corsmeier U, Van Baelen J, Behrendt A, Behrendt R, Blyth R, Coulter R, Crewell S, Di Girolamo P, Dorninger M, Flamant C, Foken T, Hagen M, Hauck C, Hoeller H, Konow H, Kunz M, Mahlke H, Mobbs SD, Richard E, Steinacker R, Weckwerth T, Wieser A, Wulfmeyer V. 2008. Mechanisms initiating deep convection over complex terrain during COPS. *Meteorol. Z.* **6**: 931–948.
- Kunz M, Kugel PSI. 2015. Detection of hail signatures from single-polarization C-band radar reflectivity. *Atmos. Res.* **153**: 565–577.
- Kunz M, Puskeiler M. 2010. High-resolution assessment of the hail hazard over complex terrain from radar and insurance data. *Meteorol. Z.* **19**: 427–439.
- Kunz M, Sander J, KC. 2009. Recent trends of thunderstorm and hailstorm frequency and their relation to atmospheric characteristics in southwest Germany. *Int. J. Climatol.* **29**: 2283–2297.
- Löffler-Mang M, Schön D, Landry M. 2011. Characteristics of a new automatic hail recorder. *Atmos. Res.* **100**: 439–446.
- McMaster HJ. 1999. The potential impact of global warming on hail losses to winter cereal crops in New South Wales. *Clim. Change* **43**: 455–476.
- Mahoney K, Alexander MA, Thompson G, Barsugli JJ, Scott J. 2012. Changes in hail and flood risk in high-resolution simulations over Colorado's mountains. *Nat. Clim. Change* **2**: 125–131.
- Mandapaka PV, Germann U, Panziera L, Hering A. 2012. Can Lagrangian extrapolation of radar fields be used for precipitation nowcasting over complex Alpine orography? *Weather and Forecasting* **27**: 28–49.
- Mandapaka PV, Germann U, Panziera L. 2013. Diurnal cycle of precipitation over complex Alpine orography: Inferences from high-resolution radar observations. *Q. J. R. Meteorol. Soc.* **139**: 1025–1046, doi: 10.1002/qj.2013.
- Manzato A. 2013. Hail in northeast Italy: Climatology and bivariate analysis with the sounding-derived indices. *Atmos. Res.* **51**: 449–467.
- Mather GK, Treddenick D, Parsons R. 1976. An observed relationship between the height of the 45-dBZ contours in storm profiles and surface hail reports. *J. Appl. Meteorol.* **15**: 1336–1340.
- Mecklenburg S, Joss J, Schmid W. 2000. Improving the nowcasting of precipitation in an Alpine region with an enhanced radar echo tracking algorithm. *J. Hydrol.* **239**: 46–68.
- Merino A, García-Ortega E, López L, Sánchez JL, Guerrero-Higuera AM. 2013. Synoptic environment, mesoscale configurations and forecast parameters for hailstorms in southwestern Europe. *Atmos. Res.* **122**: 183–198.
- Mezher RN, Doyle M, Barros V. 2012. Climatology of hail in Argentina. *Atmos. Res.* **114–115**: 70–82.
- Mohr S. 2013. 'Änderung des Gewitter- und Hagelpotentials im Klimawandel.' PhD thesis. KIT Scientific Publishing: Karlsruhe, Germany.
- Mohr S, Kunz M. 2013. Recent trends and variabilities of convective parameters relevant for hail events in Germany and Europe. *Atmos. Res.* **123**: 211–228.
- Morel S. 2014. 'Verification of radar-based hail detection algorithms with insurance loss data in Switzerland', Masters thesis. Faculty of Science, University of Bern, Switzerland.
- Morgan GM. 1973. A general description of the hail problem in the Po valley of northern Italy. *J. Appl. Meteorol.* **12**: 338–353.
- Nisi L, Ambrosetti P, Clementi L. 2014. Nowcasting severe convection in the Alpine region: The COALITION approach. *Q. J. R. Meteorol. Soc.* **140**: 1684–1699, doi: 10.1002/qj.2249.
- Panziera L, Germann U. 2010. The relation between airflow and orographic precipitation on the southern side of the Alps as revealed by weather radar. *Q. J. R. Meteorol. Soc.* **136**: 222–238, doi: 10.1002/qj.544.
- Plumondon JR. 1901. *Les orages et la grêle*. Masson et Cie: Paris (In French).
- Počakal D, Večenaj Z, Štalc J. 2009. Hail characteristics of different regions in continental part of Croatia based on influence of orography. *Atmos. Res.* **93**: 516–525.
- Puskeiler M. 2013. *Radarbasierte Analyse der Hagelgefährdung in Deutschland*, PhD Thesis. Karlsruher Institut für Technologie (KIT) Scientific Publishing: Karlsruhe, Germany. 10.5445/KSP/1000034773 (accessed 1 September 2015).
- Rinehart RE, Staggs DW, Changnon SA. 1968. Identification of hail and no-hail echoes. In *Proceedings of the 13th Radar meteorology Conference*, 20–23 August 1968. Montreal, Canada: 422–427. American Meteorological Society: Boston.
- Rotach MW, Ambrosetti P, Ament F, Appenzeller C, Arpagaus M, Bauer HS, Behrendt A, Bouvier F, Buzzi A, Corazza M, Davolio S, Denhard M, Dorninger M, Fontannaz L, Frick J, Fundel F, Germann U, Gorgas T, Hegg C, Hering A, Keil C, Liniger MA, Marsigli C, McTaggart-Cowan R, Montaini A, Mylne K RR, Richard E, Rossa A, Santos-Munoz D, Schaer C, Seity Y, Staudinger M, Stoll M, Volkert H, Walser A, Wang Y, Werhahn J, Wulfmeyer W, Zappa M. 2009. MAP D-PHASE: Real-time demonstration of weather forecast quality in the Alpine region. *Bull. Am. Meteorol. Soc.* **90**: 1321–1336.
- Šálek M, Cheze JL, Handwerker J, Delobbe L, Uijlenhoet R. 2004. 'Radar techniques for identifying precipitation type and estimating quantity of precipitation.' Document of COST Action 717, WG 1. http://www.smhi.se/cost717/doc/WDF_01_200407_1.pdf (accessed 01 September 2015).
- Saltikoff E, Tuovinen JP, Kotro J, Kuitunen T, Hohti H. 2010. A climatological comparison of radar and ground observations of hail in Finland. *J. Appl. Meteorol. Clim.* **49**: 101–114, doi: 10.1175/2009JAMC2116.1.
- Sánchez JL, Frailé R, DelaMadrid JL, DelaFuente MT, Rodríguez P, Castro A. 1996. Crop damage: The hail size factor. *J. Appl. Meteorol.* **35**: 1535–1541.
- Sánchez JL, López L, García-Ortega E, Gil B. 2013. Nowcasting of kinetic energy of hail precipitation using radar. *Atmos. Res.* **123**: 48–60.
- Schemm S, Nisi L, Martynov A, Martius O. 2016. Hail formation in pre-frontal environments: A long-term study over Switzerland. *Atmos. Sci. Lett.* In Press.
- Schuster SS, Blong RJ, Speer M. 2005. A hail climatology of the Greater Sydney Area and New South Wales, Australia. *Int. J. Climatol.* **25**: 1633–1650.
- Schuster SS, Blong RJ, McAneney KJ. 2006. Relationship between radar-derived hail kinetic energy and damage to insured buildings for severe hailstorms in eastern Australia. *Atmos. Res.* **81**: 215–235.
- Skrpničková K, Režáčová D. 2014. Radar-based hail detection. *Atmos. Res.* **144**: 175–185.

- Stucki M, Egli T. 2007. 'Synthesebericht Elementarschutzregister Hagel. Präventionsstiftung der kantonalen Gebäudeversicherungen.' http://praeventionsstiftung.ch/getmedia/da25e9c1-dfe7-465e-a04c-6c03de8fe073/Hagel_d.pdf.aspx (accessed 1 September 2015).
- Treloar ABA. 1996. Vertically integrated liquid water content as an indicator of severe hail in New South Wales. In *Preprints of 5th Australian Severe thunderstorm Conference*, 28 July–2 August 1996. Avoca Beach, New South Wales: 48–48f. Australian Bureau of Meteorology: Melbourne.
- Treloar ABA. 1998. Vertically integrated radar reflectivity as an indicator of hail size in the Greater Sydney region of Australia. In *Proceedings of 19th Conference on Severe Local Storms*, 14–18 September 1998. Minneapolis, MN: 48–51. American Meteorological Society: Boston.
- Tuovinen J, Punkka A, Rauhala J, Hohti H, Schultz D. 2009. Climatology of severe hail in Finland: 1930–2006. *Mon. Weather Rev.* **137**: 2238–2249.
- Uppala SM, Källberg PW, Simmons AJ, Andrae U, Bechtold VDC, Fiorino M, Gibson JK, Haseler J, Hernandez A, Kelly GA, Li X, Onogi K, Saarinen S, Sokka N, Allan RP, Andersson E, Arpe K, Balmaseda MA, Beljaars ACM, Berg LVD, Bidlot J, Bormann N, Caires S, Chevallier F, Dethof A, Dragosavac M, Fisher M, Fuentes M, Hagemann S, Hólm E, Hoskins BJ, Isaksen I, Janssen PAEM, Jenne R, McNally AP, Mahfouf J-F, Morcrette J-J, Rayner NA, Saunders RW, Simon P, Sterl A, Trenberth KE, Untch A, Vasiljevic D, Viterbo P, Woollen J. 2005. The ERA-40 re-analysis. *Q. J. R. Meteorol. Soc.* **131**: 2961–3012, doi: 10.1256/qj.04.176.
- Villarini G, Krajewski WF. 2010. Review of the different sources of uncertainty in single polarization radar-based estimates of rainfall. *Surv. Geophys.* **31**: 107–129.
- Vinet F. 2001. Climatology of hail in France. *Atmos. Res.* **56**: 309–323.
- Waldvogel A, Federer B, Grimm P. 1979. Criteria for the detection of hail cells. *J. Appl. Meteorol.* **18**: 1521–1525.
- Webb JDC, Elsom DM, Reynolds DJ. 2001a. Climatology of severe hailstorms in Great Britain. *Atmos. Res.* **56**: 291–308.
- Webb RM, Treloar ABA, Colquhoun JR, Potts RJ, Bally J, Keenan TD, May PT. 2001b. Overview of Sydney weather during the Forecast Demonstration Project. In *Preprints of 30th International Conference on Radar Meteorology*, 19–24 July 2001. Munich, Germany: 477–479. American Meteorological Society: Boston.
- Weisman ML, Skamarock WC, Klemp JB. 1997. The resolution dependence of explicitly modeled convective systems. *Mon. Weather Rev.* **125**: 527–548.
- Weusthoff T. 2011. Weather type classification at MeteoSwiss – introduction of new automatic classification schemes. *Arbeitsberichte der MeteoSchweiz* **235**. <http://www.meteoschweiz.admin.ch/content/dam/meteoswiss/en/Ungebundene-Seiten/Publikationen/Fachberichte/doc/ab235.pdf> (accessed 1 September 2015).
- Wieringa J, Holleman I. 2006. If cannons cannot fight hail, what else? *Meteorol. Z.* **15**: 659–669.
- Willk KE. 1961. 'Radar investigations of Illinois hailstorms.' Scientific Report No 1, Contract No. AF19(604)-4940. State Water Survey: Urbana, IL.
- Wilks DS. 2006. *Statistical Methods in the Atmospheric Sciences: An Introduction* (2nd edn). Amsterdam: Academic Press.
- Willemse S. 1995. 'A statistical analysis and climatological interpretation of hailstorms in Switzerland'. PhD thesis No. 11137. ETH Zürich: Zürich, Switzerland.
- Witt A, Eilts MD, Stumpf GJ, Johnson JT, Mitchell ED, Thomas KW. 1998. An enhanced hail detection algorithm for the WSR-88D. *Weather and Forecasting* **13**: 286–303.
- Xie BG, Zhang QH, Wang YQ. 2008. Trends in hail in China during 1960–2005. *Geophys. Res. Lett.* **35**: L13801, doi: 10.1029/2008GL034067.
- Xie BG, Zhang QH, Wang YQ. 2010. Observed characteristics of hail size in four regions in China during 1980–2005. *J. Clim.* **23**: 4973–4982.
- Zhang CX, Zhang QH, Wang YQ. 2008. Climatology of hail in China: 1961–2005. *J. Appl. Meteorol. Clim.* **47**: 795–804.